

The Pennsylvania State University

The Graduate School

Eberly College of Science

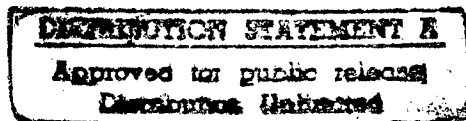
**COVARIANCE MAPPING OF AMMONIA
CLUSTERS: AN ANALYSIS TOOL OF
TIME-OF-FLIGHT MASS SPECTROMETRY**

A Research Report in

Chemistry

by

Dennis A. Card



**Submitted in Partial Fulfillment
of the Requirements
for the Degree of**

Masters of Science

May 1997

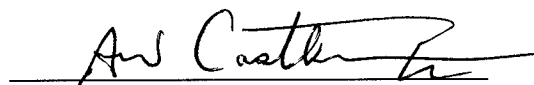
19970508 036

I grant The Pennsylvania State University the nonexclusive right to use this work for the University's own purposes and to make single copies of the work available to the public on a not-for-profit basis if copies are not otherwise available.

Dennis A. Card

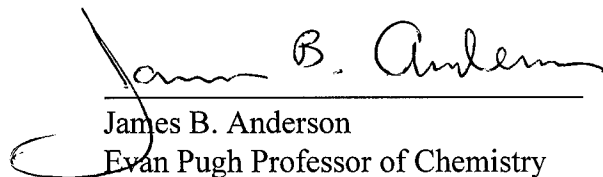
We approve the research report of Dennis A. Card

Date of Signature



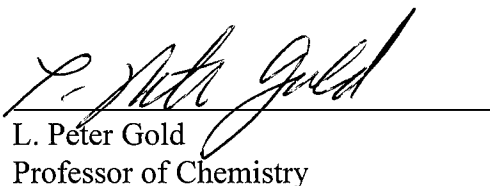
A. Welford Castleman, Jr.
Evan Pugh Professor of Chemistry
Chair of Committee
Research Advisor

March 21, 1997



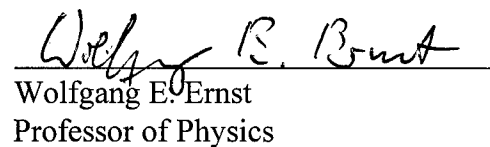
James B. Anderson
Evan Pugh Professor of Chemistry

March 21, 1997



L. Peter Gold
Professor of Chemistry

March 21, 1997



Wolfgang E. Ernst
Professor of Physics

March 21, 1997



Steven M. Weinreb
Professor of Chemistry
Head of the Department of Chemistry

March 21, 1997

ABSTRACT

Direct evidence is reported of the connectivity of charged clusters with highly charged species (N^{4+} , N^{3+} , and N^{2+}) produced upon the interaction of molecular ammonia clusters with an intense femtosecond laser beam ($\sim 10^{15}$ W/cm² at 120 fs). The value of covariance analysis as a general technique for studying dynamical processes in clusters is demonstrated through elucidating the details of various Coulomb explosion events. Positive covariance determinations identify concerted processes such as the concomitant explosion of protonated cluster ions of unsymmetrical size. Anti-covariance mapping is exploited to distinguish competitive reaction channels such as the production of highly charged nitrogen atoms formed at the expense of the protonated members of a cluster ion ensemble. This study demonstrates the great potential which covariance analysis offers in identifying the precursors and products of dynamical events in clusters, and provides further support to the ignition model as a mechanism contributing to the initial ionization events in clusters leading to highly charged atomic species.

TABLE OF CONTENTS

LIST OF FIGURES	viii
ACKNOWLEDGMENTS	x
CHAPTER 1 INTRODUCTION	1
References	3
CHAPTER 2 EXPERIMENTAL SETUP	5
2.1 Introduction	5
2.2 Colliding Pulse Mode-Locked Dye Laser	5
2.3 Amplification	9
2.3.1 Bowtie Amplifier	11
2.3.2 Bethune Cell Amplifiers	11
2.4 Recompression	13
2.5 Final Focusing and Fluence	14
2.6 Modal Characteristics	17
2.7 Timing	20
2.8 The Reflectron Time-of-Flight Mass Spectrometer (R-TOFMS)	21
2.8.1 Neutral Clusters	21
2.8.2 The Time-of-Flight Lenses	22
2.8.3 Reflectron	23
2.8.4 Microchannel Plate (MCP) Detector	25

2.9	Computations	26
2.9.1	Data Collection	26
2.9.2	Calculation of Covariance	26
2.10	References	28
CHAPTER 3	COVARIANCE MAPPING OF AMMONIA CLUSTERS: EVIDENCE OF THE CONNECTIVENESS OF CLUSTERS WITH COULOMBIC EXPLOSION	29
3.1	Introduction	29
3.2	Experimental	30
3.3	Results and Discussion	32
3.4	Conclusion	44
3.5	References	47
CHAPTER 4	FUTURE DIRECTIONS	51
4.1	Introduction	51
4.2	Proposal	51
4.2.1	Exploring the Coulomb Explosion Process	52
4.2.2	Covariance Mapping and Metastable Decay	54
4.2.3	The Kinetic Process Governing Coulomb Explosion	54
4.3	Conclusion	55
4.4	References	56
APPENDIX	COMPUTER PROGRAMS	57
A.1	Introduction	57

A.2	PASCAL Routines	57
A.2.1	Femtoscan.exe	58
A.2.2	Covar.exe	58
A.3	FORTTRAN Routines	61
A.3.1	Covar.f	61
A.3.2	Optim.f	64
A.3.3	References	66

LIST OF FIGURES

2-1	The femtosecond laser generation and amplification system.	6
2-2	The Reflectron Time-of-Flight Mass Spectrometer (R-TOFMS).	7
2-3	The colliding pulse mode-locked dye (CPM) laser.	8
2-4	The 6 pass Bowtie amplifier.	10
2-5	The Bethune cell amplifier. (a) The cross sectional view of the prism with the bore axis where the CPM beam and the sulforhodamine solution travel concurrently. Note the reflected YAG beam amplify the CPM along the bore axis from all sides. (b) The topical view of the entire cell indicating the paths of the intersecting beams.	12
2-6	Comparison of Gaussian pulse widths. Peak areas are normalized to allow a comparison of the pulse widths.	15
2-7	The normalized beam energy functions of the TEM_{00} and TEM_{10} modes. The beam intensity is plotted as the square of these functions.	19
2-8	The time-of-flight spectrum of ammonia clusters	24
3-1	Reaction schematic of the excitation of a neutral ammonia cluster to ionization. State I represents an excited state capable of inducing the Coulomb explosion process. State II is the threshold region where moieties of Coulomb exploded particles (CEPs) and singly charged clusters are seen. State III is ionized cluster state where only singly charged clusters are prevalent as products. State IV is the state in which the cohesive energy of the cluster overcomes the Coulomb repulsion caused by the charges within the cluster.	35
3-2	Covariance Map of Ammonia Clusters. The abscissa and ordinate display a TOF spectrum of ammonia clusters averaged from 10000 single shot spectra. The center of the figure displays the calculated covariance map as described in the text. Symmetry is clearly visible along the x-y axis starting in the lower left corner. Coupled species are identified by their covariance.	39

- 3-3 Anti-Covariance Map of Ammonia Clusters. The abscissa and ordinate display a TOF spectrum averaged over 10000 single shots. Proof of the competitive reaction is seen in the CEP cluster covariance field which was absent in the similar domain of Figure 3-2. Although the covariance and the anti-covariance maps appear to overlap, each data point (x,y) is distinct and is found on only one map. 41
- 3-4 Protonated ammonia ions correlated with other protonated ammonia ions. 42
Larger singly charged clusters are seen to occur less frequently with similar order singly charged species. A preference of all singly charged clusters occurring with smaller size singly charged clusters is evident. Note self correlations are removed to prevent skewing of the plot at each point.
- 3-5 Protonated ammonia clusters correlated with multicharged nitrogen ions. 45
Using the correlation coefficient, the multicharged particles are compared with singly charged cluster species without the influence of intensity. Evident is the higher anti-correlation of multicharged species with small size clusters. Although some uncertainties still exist, the peak of mass-to-charge (m/z) 2 in the time-of-flight spectrum was assigned as N^{7+} because of the similarities exhibited in this plot with the other multicharged nitrogen atoms.
- 4-1 The Reflectron Time-of-Flight Mass Spectrometer (R-TOFMS) with Mass Gate 53

ACKNOWLEDGMENTS

I would like to first acknowledge my indebtedness to Dr. A. W. Castleman, Jr. He has been without question the most patient and gracious leader I have ever had the pleasure of working for. Without his guidance, forethought, and assistance, this research would not have proceeded.

I wish also to thank the present and former members of the Castleman Group. Each has been instrumental in my development as a scientist. I would especially like to thank Dr. Steven Buzza, who introduced me to femtosecond lasers and who undoubtedly put his own career on hold during the summer of 1995 to teach me the ins and outs of the CPM laser. My thanks are equally given to Dan Folmer, Dr. Shin Sato, and Dr. Eric Snyder who were instrumental in the completion of my research. Finally, I would like to extend my sincere thanks to Barbara Itinger who eased the many administrative actions that I encountered while I was in the group.

I sincerely appreciate the assistance Don Kiel of Geo Decisions in the plotting of the covariance data. For several months, I was unable to plot all the data that I analyzed. Don volunteered his assistance and doggedly continued that assistance throughout the analysis.

The military life has been an exceptional adventure for my wife and me. The stress that this has caused my wife, Celeste, can never be measured. With little or no complaint she has endured my absence during deployments, briefs, long hours at the office, and more recently studying and preparation for tests. By remaining with me, she has dealt with the separation from parents, siblings, and grandparents - ultimately with the deaths of her brother who

passed away in February 1995 and her grandmother who passed away in March 1995. I thank her for her patience, love, support, and understanding.

I thank each of my children - Sarah, Adam, Hannah, and Rachel - for the gentle patience they have had waiting for their father, for the many hours we have spent apart, and for the lost friends from our many moves. I pray they may learn from their experiences and grow from these difficulties.

My gratitude extends also to my parents, Leon and Laura Card. They not only brought me into this world, but also instilled in me determination, confidence, and discipline. Although they probably understood little of my education from the eighth grade on, they supported me unfailingly.

I am also indebted to my father-in-law and mother-in-law, Norman and Kathy Porath. They have always been warm and understanding - integrating me into their family seemingly like one of their own children. I am always amazed at the new facet of life I am exposed to when I visit them.

Finally, I thank God for answering my prayers, for keeping my family safe, and for the many blessings I have been given.

Chapter 1

Introduction

The study of clusters and their time dependence has been under considerable scrutiny for a number of years. An early focus was the gas condensed phase transition¹⁻⁶. The advent of the laser and the production of clusters via supersonic expansion coupled with the renaissance of the time-of-flight mass spectrometer, introduced a new dimension for exploring the time dynamics of clusters¹⁻⁶. Recently, the dynamics of clusters opened a new chapter with the discovery of a connection of multicharged atoms with clusters.⁷⁻¹³

The study of clusters produced via supersonic expansion proceeded with an acknowledged problem - that of an unknown parent reactant. Clusters are typically produced through a pulsed nozzle with a variable internal diameter and opening duration, leading to a wide distribution of sizes. Because of the problem of cluster fragmentation during detection, the exact composition of the neutral cluster has remained unknown.

The visionary work of covariance mapping on simple molecules by Codling, et al. has shown an unambiguous identification of these species¹⁴⁻²². The success of this technique in the case of small molecules has suggested that a similar approach to clusters would be meaningful. Extending this technique to clusters has opened the opportunity to determine the identity of the reactant species and to better understand reactions in cluster systems.

The mechanism involving clusters in the production of multicharged ions has been under considerable scrutiny. The current debate essentially involves the symmetry of the dissociation when clusters interact with intense laser fields²³. Two models to explain the mechanism, the coherent electron motion model (CEMM)¹¹ and the ionization ignition mechanism (IIM)¹², have advanced to the forefront of the debate. In the CEMM, the charge on the cluster comes to equilibrium forming a coherent field, allows subsequent electrons to be removed similar to electron impact ionization, and results in a symmetric breakage of the cluster. In the IIM, the charge on the cluster is unsymmetric forming an inhomogenous field and results in an unsymmetric breakage of the cluster.

The recent work by the Corkum and Bandrauk groups have advanced a theory which seems to further explain the IIM²³⁻²⁶. Multiple ionization is found to exist when charge resonant states are strongly coupled because the interaction of a species with an intense laser. Electron localization near one nucleus causes an instantaneous Stark effect which suppresses electron tunneling and lowers the potential barrier of one charge state. The resultant system allows a cascading of electrons into the continuum of the suppressed potential well and explains the large ionizations which are seen to occur in intense laser fields.

The focus of this work has been to develop the computational means of producing covariance maps. Using ammonia clusters, covariance maps will be seen in Chapter 3 to infer the reactant composition. Additionally, insight into the debate of Coulomb explosion symmetry will be presented.

References

1. A. W. Castleman, Jr., *J. of Cluster Sci.* **1**, 3 (1990).
2. A. W. Castleman, Jr., *Int. J. of Mass Spectr. and Ion Proc.* **118/119**, 167 (1992).
3. A. W. Castleman, Jr., S. Wei, *Annu. Rev. Phys. Chem.* **45**, 685 (1994).
4. A. W. Castleman, Jr., in *Clusters of Atoms and Molecules II*, ed. H. Haberland, Springer-Verlag, Berlin, 77 (1994).
5. J. A. Syage, in *Femtosecond Chemistry*, ed. J. Manz and L. Wöste, VCH Verlagsgesellschaft mbH, Weinheim, 475 (1995).
6. A. W. Castleman, Jr., K. H. Bowen, Jr., *J. Phys. Chem.* **100**, 12911 (1996).
7. J. Purnell, E. M. Snyder, S. Wei, A. W. Castleman, Jr., *Chem. Phys. Lett.* **229**, 333 (1994).
8. E. M. Snyder, S. Wei, J. Purnell, S. A. Buzza, A. W. Castleman, Jr., *Chem. Phys. Lett.* **248**, 1 (1996).
9. E. M. Snyder, D. A. Card, D. E. Folmer, A. W. Castleman, Jr. in *Resonant Ionization Spectroscopy 1996*, ed. N. Winograd and J. E. Parks, American Institute of Physics, Woodbury, 379 (1997).
10. E. M. Snyder, S. A. Buzza, A. W. Castleman, Jr., *Phys. Rev. Lett.* **77**(16), 3347 (1996).
11. K. Boyer, B. D. Thompson, A. McPherson, C. K. Rhodes, *J. Phys. B: At. Mol. Opt. Phys.* **27**, 4373 (1994).
12. C. Rose-Petruck, K. J. Schafer, C. P. Barty, *J. Applications of Laser Plasma Radiation II, SPIE* **272**, 2523 (1995).
13. I. Last, I. Schek, J. Jortner, *Energetics and Dynamics of Coulomb Explosion of Highly Charged Clusters*, To be published.
14. P. A. Hatherly, L. J. Frasinski, K. Codling, A. J. Langley, W. Shaikh, *J. Phys. B: At. Mol. Opt. Phys.* **23**, L291 (1990).

15. P. A. Hatherly, M. Stankiewicz, K. Codling, L. J. Frasinski, G. M. Cross, *J. Phys. B: At. Mol. Opt. Phys.* **27**, 2993 (1994).
16. L. J. Frasinski, M. Stankiewicz, P. A. Hatherly, G. M. Cross, K. Codling, A. J. Langley, W. Shaikh, *Phys. Rev. A* **46**, R6789 (1992).
17. L. J. Frasinski, K. Codling, P. A. Hatherly, *Phys. Lett. A* **142**, 499 (1989).
18. L. J. Frasinski, P. A. Hatherly, K. Codling, *Phys. Lett. A* **156**, 227 (1991).
19. L. J. Frasinski, P. A. Hatherly, K. Codling, M. Larsson, A. Persson, C-G. Wahlström, *J. Phys. B: At. Mol. Opt. Phys.* **27**, L109 (1994).
20. L. J. Frasinski, K. Codling, P. A. Hatherly, *Science* **246**, 1029 (1989).
21. K. Codling, L. J. Frasinski, *J. Phys. B: At. Mol. Opt. Phys.* **26**, 783 (1993).
22. K. Codling, L. J. Frasinski, *Contemporary Phys.* **35**, 243 (1994).
23. T. Zuo, A. D. Bandrauk, *Phys. Rev. A* **52**(4), 1 (1995).
24. H. Stapelfeldt, E. Constant, P. B. Corkum, *Phys. Rev. Lett.* **74**(19), 3780 (1995).
25. T. Seideman, M. Y. Ivanov, P. B. Corkum, *Phys. Rev. Lett.* **75**(15), 2819 (1995).
26. E. Constant, H. Stapelfeldt, P. B. Corkum, *Phys. Rev. Lett.* **76**(22), 4140 (1996).

Chapter 2

Experimental Setup

2.1 Introduction

The equipment used in these studies is a femtosecond laser ionization source (Figure 2-1) coupled to a reflectron time-of-flight (TOF) mass spectrometer (Figure 2-2). A femtosecond pulse train is created in a colliding pulse mode-locked dye laser (CPM) pumped by a continuous wave (CW) argon ion laser. Amplification is achieved using the second harmonic of a Nd:YAG laser focused into a six pass Bowtie amplifier and a series of three Bethune cells. Recompression of the temporal width of the optical pulse is accomplished with gratings. The laser beam is focused into a mass spectrometer which ionizes a packet of neutral ammonia clusters within a TOF lens assembly patterned after the Wiley-McLaren design¹. The ionized cluster packet is accelerated out of the TOF lenses by a voltage gradient placed on the lenses. Ionized particles which remain intact are deflected by a reflectron located 1.397 m from the lens assembly, and detected by a microchannel plate detector (MCP) located 0.724 m from the reflectron. An oscilloscope measures the changes in voltage at the MCP and a personal computer records the digitized measurements.

2.2 Colliding Pulse Mode-Locked Dye Laser

A femtosecond pulse is generated via a CPM laser (Clark Instrumentation) which is shown in Figure 2-3. All lines of a 5 watt Innova 305 argon ion CW laser (Coherent) are

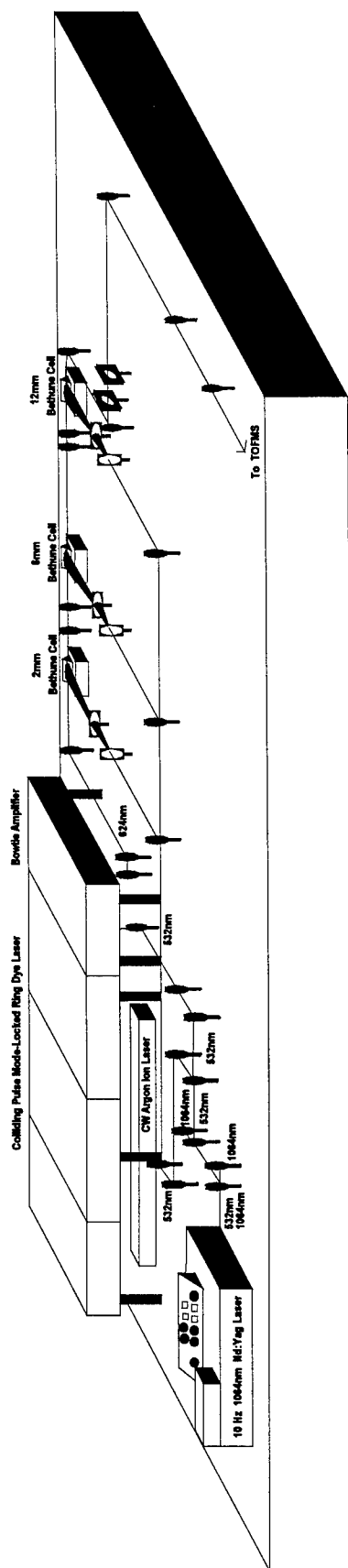


Figure 2-1. The femtosecond laser generation and amplification system.

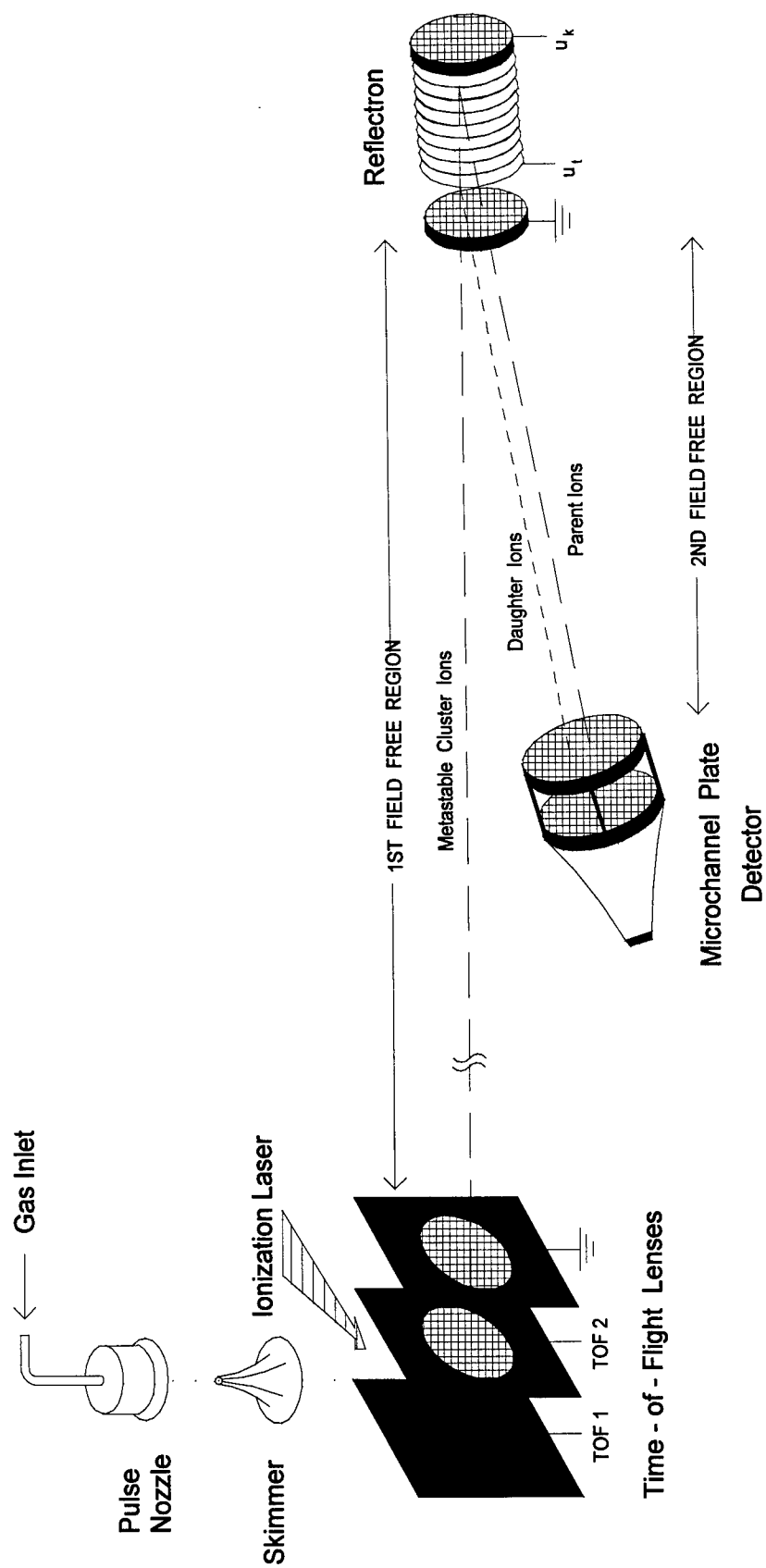


Figure 2-2. The Reflectron Time-of-Flight Mass Spectrometer (R-TOFMS).

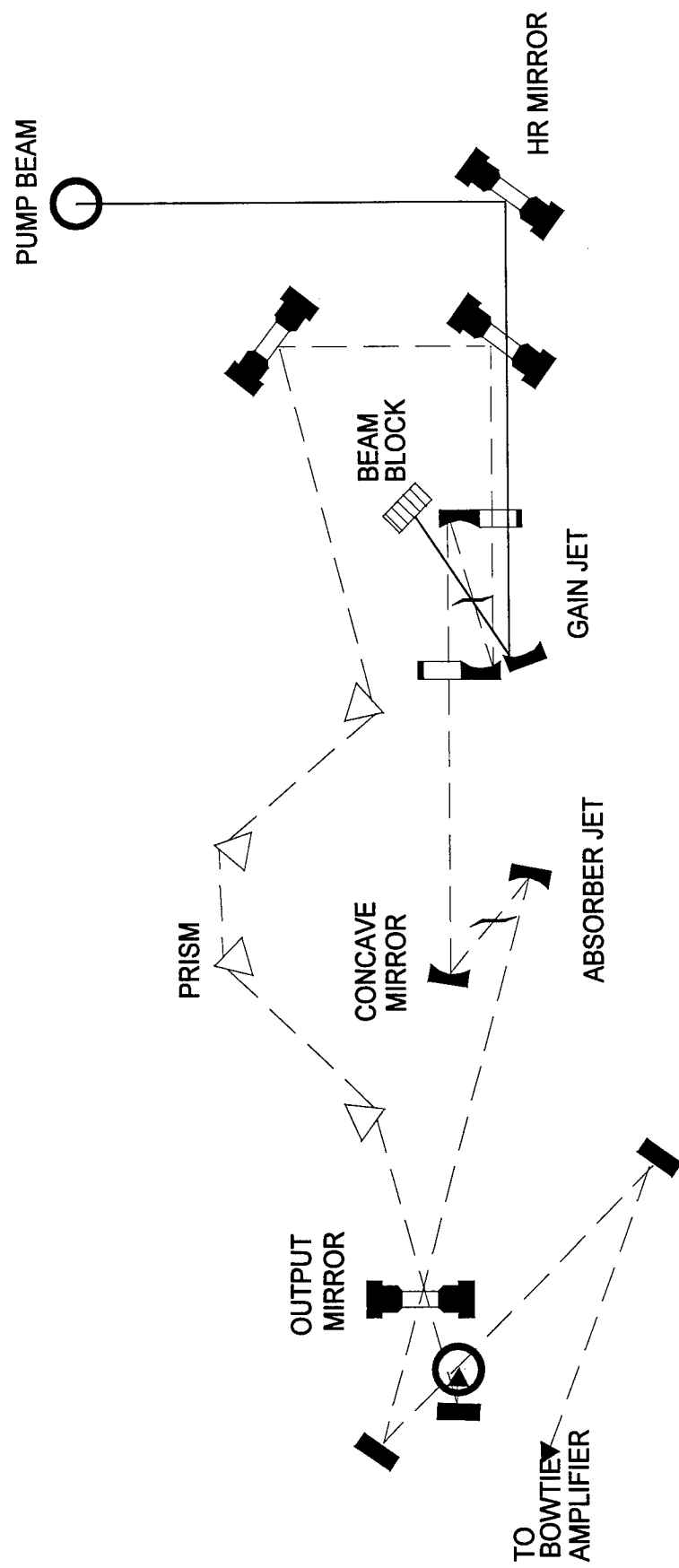


Figure 2-3. The colliding pulse mode-locked dye (CPM) laser.

focused into the gain dye jet which is pumped at approximately 42 pounds per square inch. The dye is a solution of rhodamine 590 tetrafluoroborate (Exciton) dissolved in ethylene glycol. The gain dye fluoresces in two directions, clockwise and counter-clockwise in a ring arrangement. When these two fluorescent spots overlap each other at a focus in the gain dye jet, a CW laser beam is emitted. A saturable absorber dye jet placed in the ring passively mode-locks the beam. The dye is pumped at about 17 psi. The dye, DODC Iodide (3-Ethyl-2-[5-(3-ethyl-2(3H)-benzothiazolydene)-1,2-pentadienyl] (Exciton), is dissolved in ethylene glycol. Finally, four prisms are placed in the ring to apply negative group velocity dispersion (GVD) and compress the pulse width². The wavelength of the 90 MHz beam is 624 nm and the pulse width is autocorrelated and determined to be approximately 100 fs. For the CPM, the beam is measured using a digital Model 835 Optical Power Meter (Newport Corporation) and found to be about 300 pJ.

2.3 Amplification

Amplification is achieved through two systems, a BTA-1S Bowtie amplifier (Clark Instrumentation) and Bethune cell amplifiers (Santa Ana Lasers). The first amplifies the power by approximately six orders of magnitude and the second by about three orders of magnitude. Both amplification systems rely on the second harmonic (532 nm) of a Quanta-Ray 6300 GCR 10 Hz Nd:YAG laser (Spectra Physics) transmitting energy through a dye solution of sulforhodamine 640 (Kodak) in approximately 50% methyl alcohol and water.

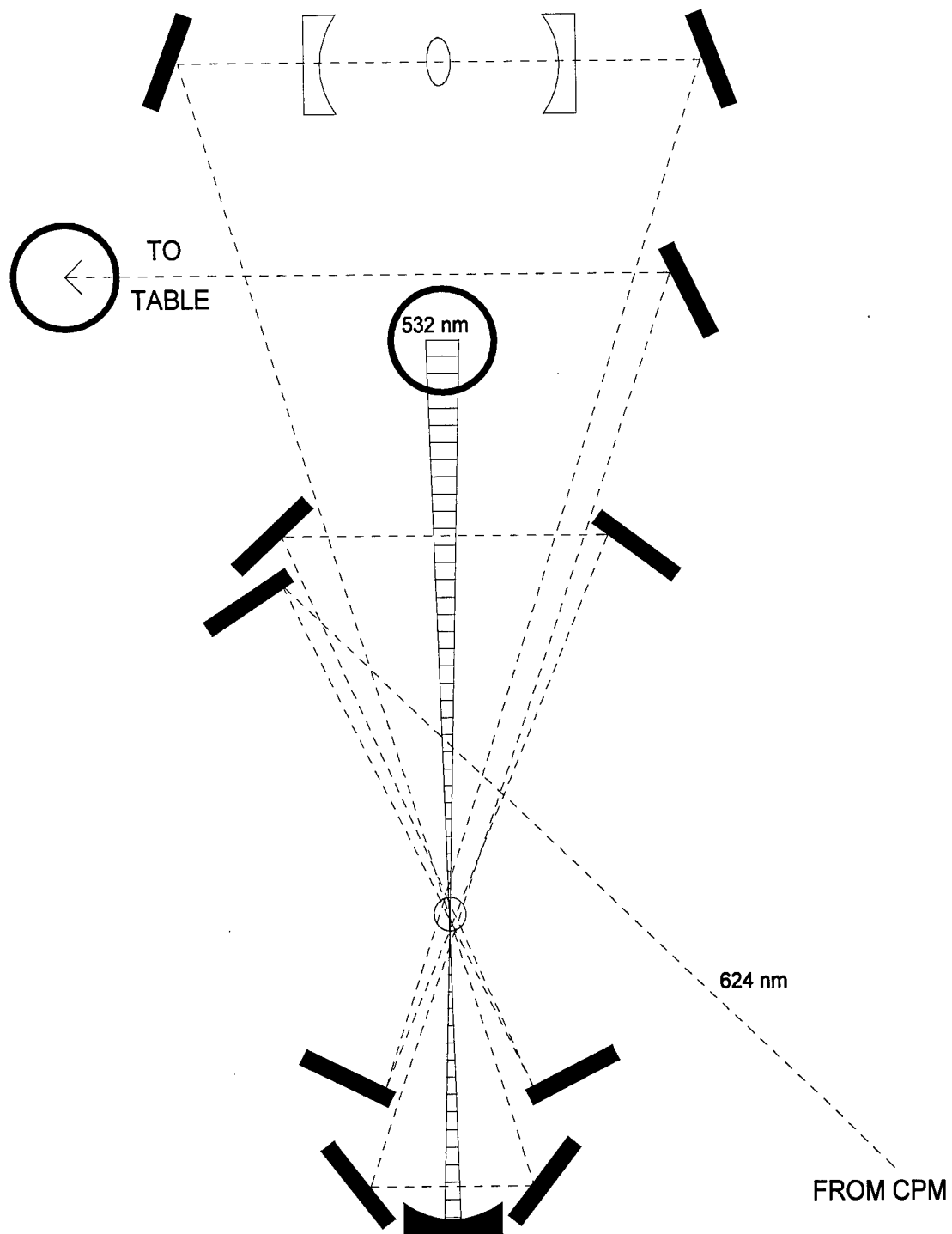


Figure 2-4. The 6 pass Bowtie amplifier.

2.3.1 Bowtie Amplifier

As shown in Figure 2-4, this amplifier is named a "bowtie" because of its general appearance. The beam from the CPM cell enters the Bowtie and is reoriented through a thin transparent tube in which the sulforhodamine solution is pumped at a pressure of about 5 psi. The beam makes a total of six passes through this tube. Five percent of the YAG output is gleaned from the main and focused through the transparent tube as well. After the YAG beam passes through the tube, it encounters a concave mirror which refocuses the beam back through the lens onto its path of origin with the focal point being within the transparent tube.

The Bowtie also has a dye jet which the beam intersects between the fourth and fifth passes through the transparent tube. This dye jet contains a solution of malachite green oxalate (Kodak) in ethylene glycol. The purpose of this jet is to reduce the amount of amplified spontaneous emission (ASE) which arises because of the excitation of sulforhodamine 640 by the YAG beam.

After all six passes, the beam is about 10 μJ per pulse with 5-10% ASE and a repetition rate of 10 Hz. The pulse width is around 150 fs. All beams including and subsequent to the Bowtie amplifier were measured using a J3 Pyroelectric Joulemeter (Molelectron) coupled to a Model 7200 oscilloscope (LeCroy).

2.3.2 Bethune Cell Amplifiers

Three Bethune cell amplifiers were used in these experiments. They are classified by the bore diameter and an example is shown in Figure 2-5. For these studies, a 2mm, a 6mm, and a 12mm cell set were used. The cell consists of a long prism in which the interior is bored to allow a sulforhodamine 640 dye to flow. A set of Brewster's

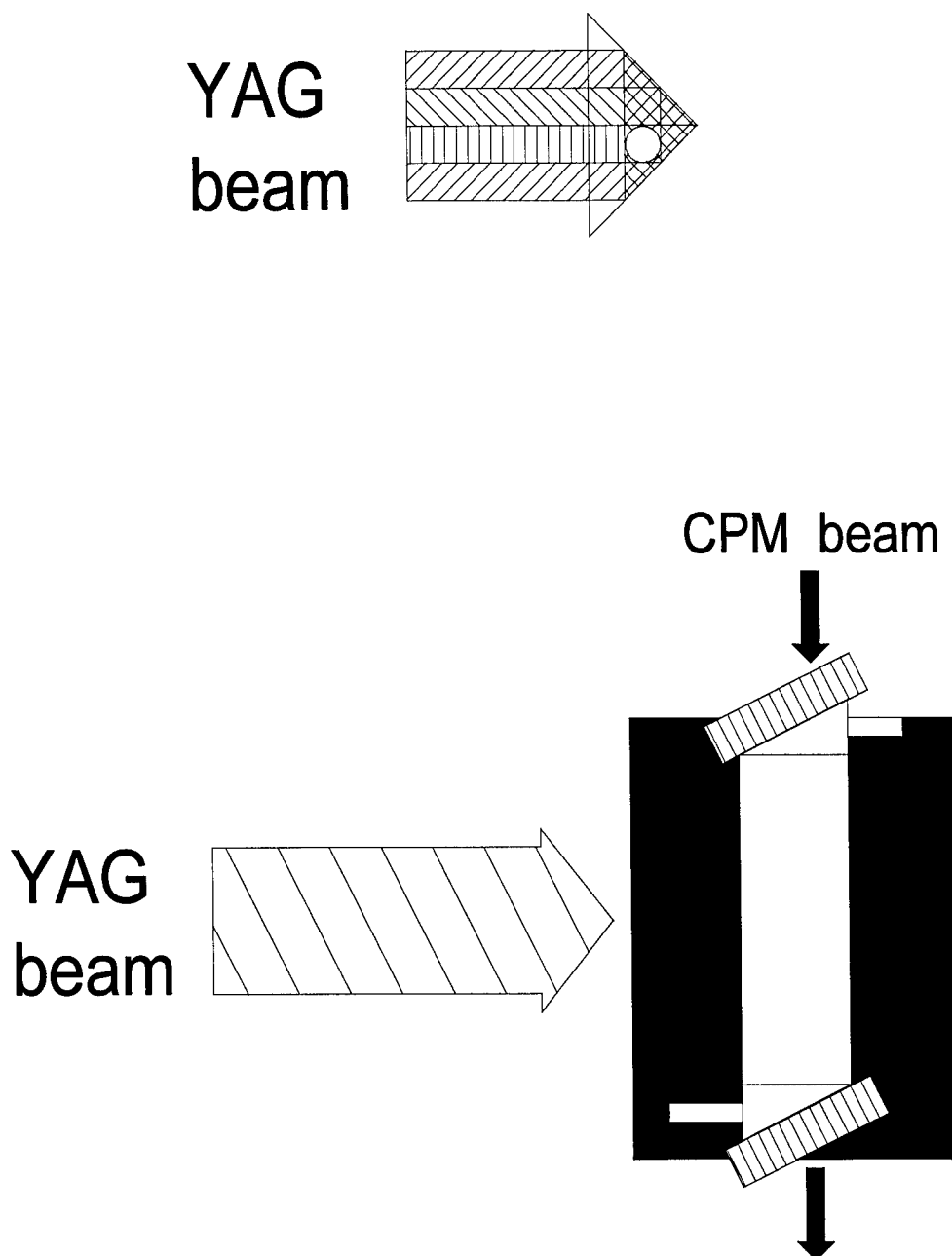


Figure 2-5. The Bethune cell amplifier. (a) The cross sectional view of the prism with the bore axis where the CPM beam and the sulforhodamine solution travel concurrently. Note the reflected YAG laser beam amplifies the CPM along the bore axis via uniform pumping from all sides (b) The topical view of the entire cell indicating the paths of the intersecting beams.³

windows, one on each side, permits a beam to pass through the bore and be amplified. An off-center bore arrangement is used such that the YAG laser beam uniformly pumps the CPM beam from all sides.

The beam measures about 2.0-2.5 mJ per pulse with about 10% ASE. The repetition rate of the beam remains at 10 Hz and without recompression the beam pulse width typically broadens to around 350 fs.

2.4 Recompression

Recompression is essential to regain peak power and a narrow time profile in the overall beam. Although amplification is assisted by longer pulse widths, ionization is not. Longer pulse widths are caused by broadening of the group pulse - thus GVD. To understand this concept, the variables influencing the change should be considered.

The change in the pulse width is given by the expression⁴,

$$\Delta\tau = \frac{2L}{c} \left[\frac{n_1 n_2 c^3}{\omega^3 n_1^3} (l + m + 1) - \frac{dn}{d\omega} \right] \Delta\omega$$

where $\Delta\tau$ is the change in the pulse width (sec)

L is the path length through the change in refractive index (m)

c is the speed of light (2.998×10^8 m/sec)

n_i is the index of refraction of material i

l and m are the mode characteristics

ω is the frequency (sec^{-1})

As can be quickly observed, the beam should broaden if the medium length is quite large, the index of refraction increases, or the frequency changes. Since the medium length

considered is quite short, the path length variable is insignificant. The index of refraction, on the other hand, increases when the beam passes from air through a lens or dye solution. Since a frequency change is indiscernible and the broadening is about 3 times, the change in the index of refraction must be the main cause.

The preceding equation assumes that the beam enters another medium perpendicular to the direction of propagation. If the entrance angle is less than 90° , the change in length through the media also must be considered. Essentially, the difference causes the highest intensity portion of the beam to remain in the media longer than the lower intensity portion of the beam. Gratings and prisms make use of this difference to apply negative GVD or recompression.

The pulse full width at half maximum (FWHM) is the reference point of measurement for pulses. Figure 2-6 shows a comparison of compressed and uncompressed beams using this standard. Each curve is a gaussian normalized in area and relative in height to the 50 fs curve. The intensity increases three times from 350 fs to 120 fs for our experiment. This peak increase serves to increase the peak pulse power by the same factor and the total power per pulse, albeit considerably less than the peak power.

Prisms were used within the CPM and a grating set were used between the 2 mm and 6 mm Bethune cells. The pulse width was 120 fs with recompression and 350 fs without.

2.5 Final Focusing and Fluence

The last step outside of the TOFMS is focusing using a 50 cm or 60 cm convex lens. The lens is readily positioned on a sliding rail and translated to focus the laser beam in between the TOF lenses to precisely intersect the pulsed cluster. When focused, the beam reduces down to a minimal diameter which can be calculated from the following

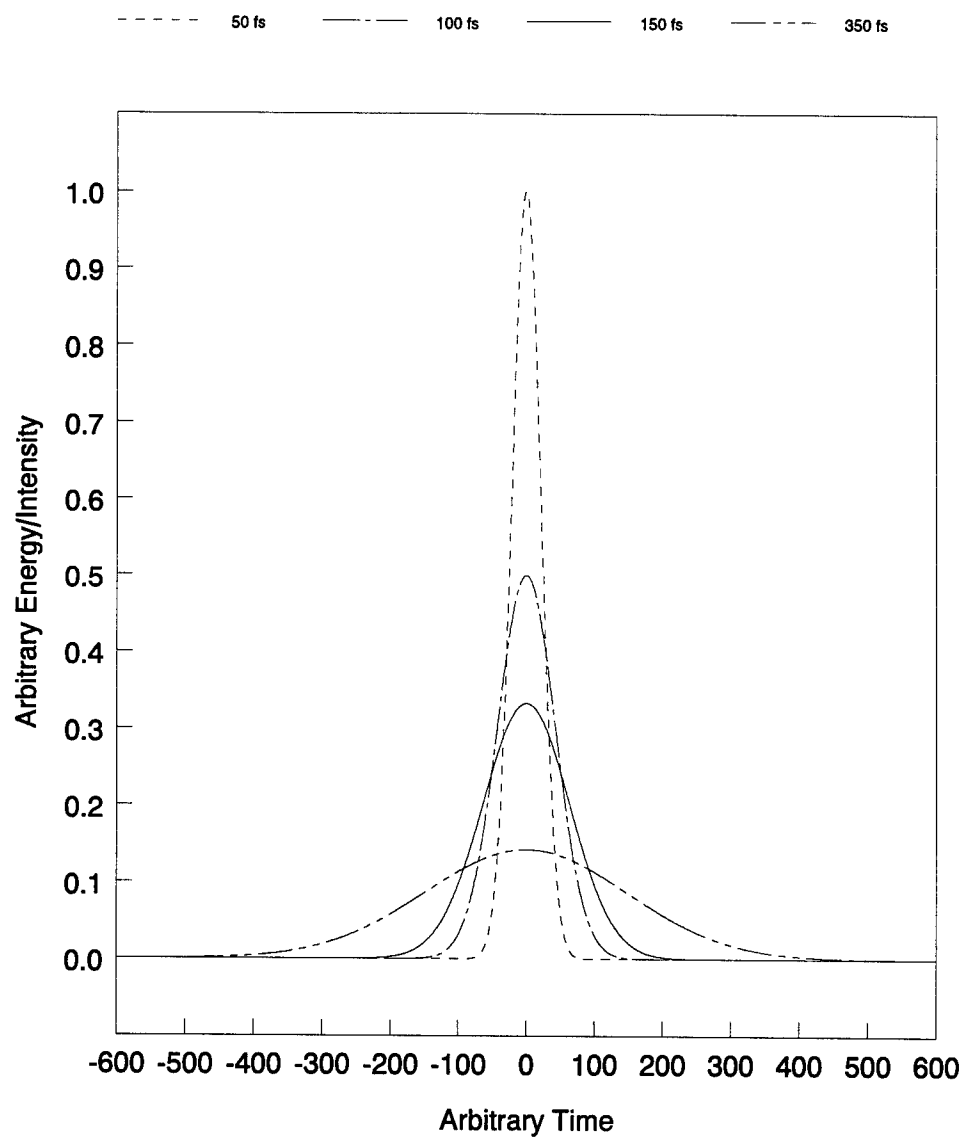


Figure 2-6. Comparison of Gaussian pulse widths. Peak areas are normalized to allow a comparison of the pulse widths.

expression⁵,

$$d = \frac{f\lambda}{\pi\omega_0 n \sqrt{1 + (f\lambda / \pi\omega_0^2 n)^2}}$$

where d is the minimal beam waist or radius (m)

f is the focal length of the lens (m)

λ is the wavelength of the light (m)

n is the index of refraction of the focal medium

ω_0 is the beam waist entering the lens (m)

Using this equation with a 60 cm focal lens with an index of refraction of 1.5, the beam area at the focal point would be $1.377 \times 10^{-6} \text{ cm}^2$.

The fluence is given by,

$$F = \frac{P}{A} = \frac{E/t}{A}$$

where F is the fluence (W/cm^2)

E is the energy per pulse (J)

P is the total power per pulse (W)

A is the focused beam area (cm^2)

t is the time per pulse (sec)

From the measured energy per pulse after the 12mm Bethune cell of approximately 2.0 mJ per pulse, the calculated power per pulse is $5 \times 10^9 \text{ W}$ per pulse with the total time per pulse of 400 fs for a 120 fs pulse width (see Figure 2-6). The fluence for the beam would then be around $3.6 \times 10^{15} \text{ W}/\text{cm}^2$ for a 120 fs pulse width. If the pulse width were

350 fs, the fluence would be about 1.6×10^{15} W/cm² or roughly half the fluence of the 120 fs beam.

2.6 Modal Characteristics

In section 2.4, the pulse width was compared as a function of time for a perfect Gaussian or a Transverse Electro-Magnetic 00 (TEM₀₀) mode. The TEM₀₀ mode is achieved in these studies, however further insight into the reasons this mode is desired can be seen by examining the modal characteristics of the energy.

Regardless of the medium, the modal characteristics develop because of the Hermitian dependence of the energy. In a homogenous medium, the energy at any position x, y, and z is defined by⁶:

$$E_{l,m}(x,y,z) = E_0 \cdot \left(\frac{\omega_0}{\omega(z)} \right) \cdot H_l \left(\frac{x\sqrt{2}}{\omega(z)} \right) \cdot H_m \left(\frac{y\sqrt{2}}{\omega(z)} \right) \cdot \exp \left[-\frac{x^2 + y^2}{\omega^2(z)} - \frac{ik(x^2 - y^2)}{2 \cdot R(z)} - ikz + i(1 + m + l) \cdot \eta \right]$$

$$\text{where } \eta = k \cdot z - (1 + m + l) \cdot \tan^{-1} \left(\frac{z}{z_0} \right)$$

$$z_0 = \frac{\pi \cdot \omega_0^2 \cdot n}{\lambda} \quad (\text{confocal beam parameter, m})$$

$$\omega^2(z) = \omega_0^2 \left(1 + \frac{z^2}{z_0^2} \right) \quad (\text{beam diameter at some distance } z, \text{ m})$$

$$R(z) = z \cdot \left(1 + \frac{z_0^2}{z^2} \right) \quad (\text{wavefront radius at some distance } z, \text{ m})$$

$$k = \frac{2 \cdot \pi \cdot n}{\lambda} \quad (\text{m}^{-1})$$

l, m are the modal parameters

n is the index of refraction of the media

λ is the wavelength of light being considered (m)

x , y , and z are the positional variables (m)

$H_{l,m}(x,y,\omega(z))$ is a Hermitian polynomial function

The Hermitian polynomial is defined as⁷:

$$H_l(y) = (-1)^l \cdot \exp(y^2) \cdot \frac{d^l \exp(-y^2)}{dy^l}$$

where y is some independent variable.

To compare the beam modes, the cross section of the beam profile will be used and the positional variable z will be set to 0. The Hermitian polynomials for 0 and 1, $H_0(y)$ and $H_1(y)$, are 1 and $-2y$, respectively. The resultant energy profiles are:

$$E_{l,m}(x, y, z) = E_{0,0}(x, y, 0) = E_0 \cdot \exp\left[-\frac{x^2}{\omega^2(0)}\right] \cdot \exp\left[-\frac{y^2}{\omega^2(0)}\right]$$

$$E_{l,m}(x, y, z) = E_{1,0}(x, y, 0) = E_0 \cdot \left(\frac{x \cdot 2\sqrt{2}}{\omega(0)}\right) \cdot \exp\left[-\frac{x^2}{\omega^2(0)}\right] \cdot \exp\left[-\frac{y^2}{\omega^2(0)}\right]$$

These two profiles are plotted at $y=0$, in Figure 2-7. TEM_{00} would result in a beam cross section of a single circle with the highest beam energy at the center. A line of symmetry would be found down the z axis. However, TEM_{10} would result in a beam cross section of two small ellipses antisymmetric around the x axis and symmetric around the y axis.

The cross sectional areas of TEM_{00} and TEM_{10} are $5.0132 \omega_0^2$ and $3.1416 \omega_0^2$, respectively. Because the fluence is inversely proportional to the area, the fluence of the TEM_{00} beam would be 50% greater than the TEM_{10} beam. Figure 2-6 also illustrates that

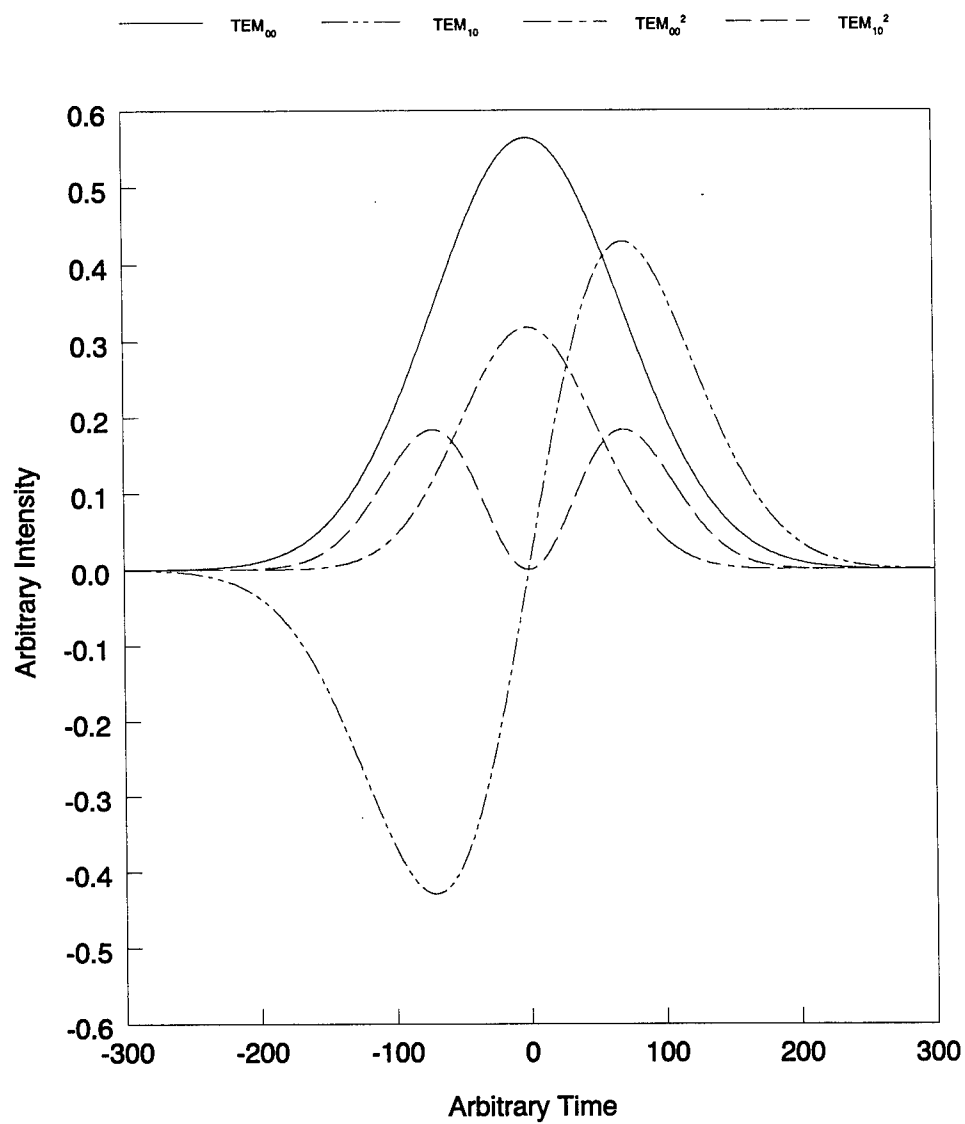


Figure 2-7. The normalized beam energy functions of the TEM_{00} and TEM_{10} modes. The beam intensity is plotted as the square of these functions.

the TEM_{10} beam has a node where the beam energy is 0. This implies that the single laser beam is split and a further decrease in the fluence would result if only half of the beam were impinged on the neutral cluster and half of the beam missed the cluster. Higher order modes would only exacerbate this problem.

In this study, good mode quality was desirable for achieving high fluence. However when kinetic energy release is studied, the mode also has implications regarding the calculations employed to deduce the various magnitudes. The TEM_{00} mode is imperative with these calculations.⁸

2.7 Timing

Timing is of paramount importance in these studies. The purpose of gaining a short pulse of high power would be meaningless if the amplified pulse missed the neutral clusters. Neither would maximum amplification of specific pulses in the pulse train occur if different pulses within the pulse train were amplified.

To ensure maximum overlap of the YAG and the CPM laser beams, path length additions and time delays are used. A photodetector, which is the same distance from the CPM output coupler as the first amplification cycle in the Bowtie, detects the CPM beam. The photodetector is connected to a BTA-1S Nanosecond Delay (Clark Instrumentation) which controls the Q-switch within the YAG. The energy as measured on the joulemeter-oscilloscope system is optimized with this delay (1-15 nsec). A physical delay is set elongating the YAG beam path to the Bethune cells in order to allow the amplified CPM peak to reach the Bethune cell at the appropriate time to achieve amplification.

The delay between the CPM beam and the pulse nozzle is controlled by a Model DG535 Four Channel Digital Delay/Pulse Generator (Stanford Research). A photodiode (Thor Lab), used as a system trigger, detects the YAG pulse just after it has been doubled

in wavelength. The delay generator controls the time when the pulse nozzle is fired and how long it stays open. The trace intensity monitored on the oscilloscope is used to optimize this delay.

2.8 The Reflectron Time-of-Flight Mass Spectrometer (R-TOFMS)

As seen in Figure 2-2, the R-TOFMS system consists of an inlet source for the species studied, a reflectron, and a means of detection.

Ionization of the species under study occurred in a vacuum environment which is maintained around 7×10^{-6} Torr by a 15 inch diffusion pump (Varian). The source pressure varied depending on the length of the pulse of the nozzle. Detection occurred in another vacuum region which is normally at 1×10^{-7} Torr. This pressure is maintained by an 18 inch diffusion pump (Varian). Pressures in both regions were detected via thermocouple gauges and read by a 307 Vacuum Gauge Controller (Granville-Phillips).

2.8.1 Neutral Clusters

The neutral clusters studied in the present work were formed by supersonic expansion⁹ through a jet nozzle into a vacuum environment. The rapid expansion into a vacuum effects substantial cooling, lowering the translational, rotational, and vibrational energies of the cluster¹⁰. Weak van der Waals bonds are formed which keep the cluster together.

In this study, neat ammonia (MG Industries, 99.98% minimum purity) was pulsed through a nozzle (General Valve Series 9) affixed with a 750 μm orifice. The ammonia was backed at about 2200 Torr and entered a vacuum chamber at 7×10^{-6} Torr. Although the maximum cluster size was never exactly known, ammonia clusters have been reported

in the ionized state with over 80 monomer units¹¹. In this study, the detected cluster size did not exceed about 15 monomer units.

2.8.2 The Time-of-Flight Lenses

Neutral clusters are ionized in the center of a set of two positively charged plates with a potential difference. This potential difference creates a gradient reflecting ionized clusters toward a lower voltage and ultimately toward the ion detector.

The TOF Lenses are portrayed in Figure 2-2. These lenses are made of solid stainless steel, 5.08 cm square and 0.3175 cm thick. TOF 2 and TOF 3 have 1.27 cm circular holes overlaid with nickel mesh. Each TOF lens is exactly 1 cm apart. TOF 1 and TOF 2 are electrified with TOF 1 having the highest voltage. TOF 3 is grounded. In this study, TOF 1 and TOF 2 were held at approximately 3600 V and 2000 V, respectively.

The nickel mesh allows a uniform voltage to be applied over the entire lens. Ionization at a selected point with a constant voltage gradient between the TOF lenses leaves each ionized species with the same kinetic energy¹¹. Using the reflectron as an energy analyzer, the birth potential (U_0) of the species may be determined. Since the voltage is uniform, the exact position of the ionization may be determined. The flight times of the species can then be calculated. They are given by:

$$t_{0 \rightarrow \text{TOF2}} = \sqrt{\frac{2 \cdot m \cdot (x_2 - x_0)(x_2 - x_1)}{q \cdot (U_1 - U_2)}}$$

$$t_{\text{TOF2} \rightarrow \text{TOF3}} = \frac{(x_3 - x_2)}{(U_2 - U_3)} \left\{ \sqrt{\frac{2 \cdot m \cdot (U_1 - U_2)(x_2 - x_0)}{q \cdot (x_2 - x_1)} + \frac{2 \cdot m \cdot (U_2 - U_3)}{q}} \right. \\ \left. - \sqrt{\frac{2 \cdot m \cdot (U_1 - U_2)(x_2 - x_0)}{q \cdot (x_2 - x_1)}} \right\}$$

$$t_{\text{drift}} = \frac{l_{\text{drift}}}{\frac{q \cdot (U_2 - U_3) \cdot t_{\text{TOF2} \rightarrow \text{TOF3}}}{m \cdot (x_3 - x_2)} + \sqrt{\frac{2 \cdot q \cdot (U_1 - U_2)(x_2 - x_0)}{m \cdot (x_2 - x_1)}}}$$

where t_i is the flight time (sec)

U_i is the potential at the TOF lens (V)

x_i is the distance from TOF 1 with respect to the lenses (m)

q is the charge of the ion (1.602×10^{-19} C)

m is the mass of the ion (kg)

If U_0 were 2800 V which would put x_0 equidistant between TOF 1 and TOF 2, $t_{0 \rightarrow \text{TOF2}}$, $t_{\text{TOF2} \rightarrow \text{TOF3}}$, and t_{drift} would equal 0.105 μsec , 0.073 μsec , and 12.062 μsec , respectively for the NH_3^+ ion. The total flight time would then be 11.240 μsec which compares closely with a flight time shown in Figure 2-8 (12.270 μsec).

As noted in Section 2.5, the laser beam is focused to an area of $1.377 \times 10^{-6} \text{ cm}^2$ which translates to a radius of $6.62 \times 10^{-4} \text{ cm}$. Since the laser ionizes the neutral cluster between TOF 1 and TOF 2, the equation for $t_{0 \rightarrow \text{TOF2}}$ can be used to calculate the time that the ion would take to move out of the beam waist. The time for a NH_3^+ ion to move away from the center of the beam is 3.82 nsec which is considerably longer than the pulse duration.

2.8.3 Reflectron

After the ions depart the TOF lenses, they traverse a field free region of 1.397 m

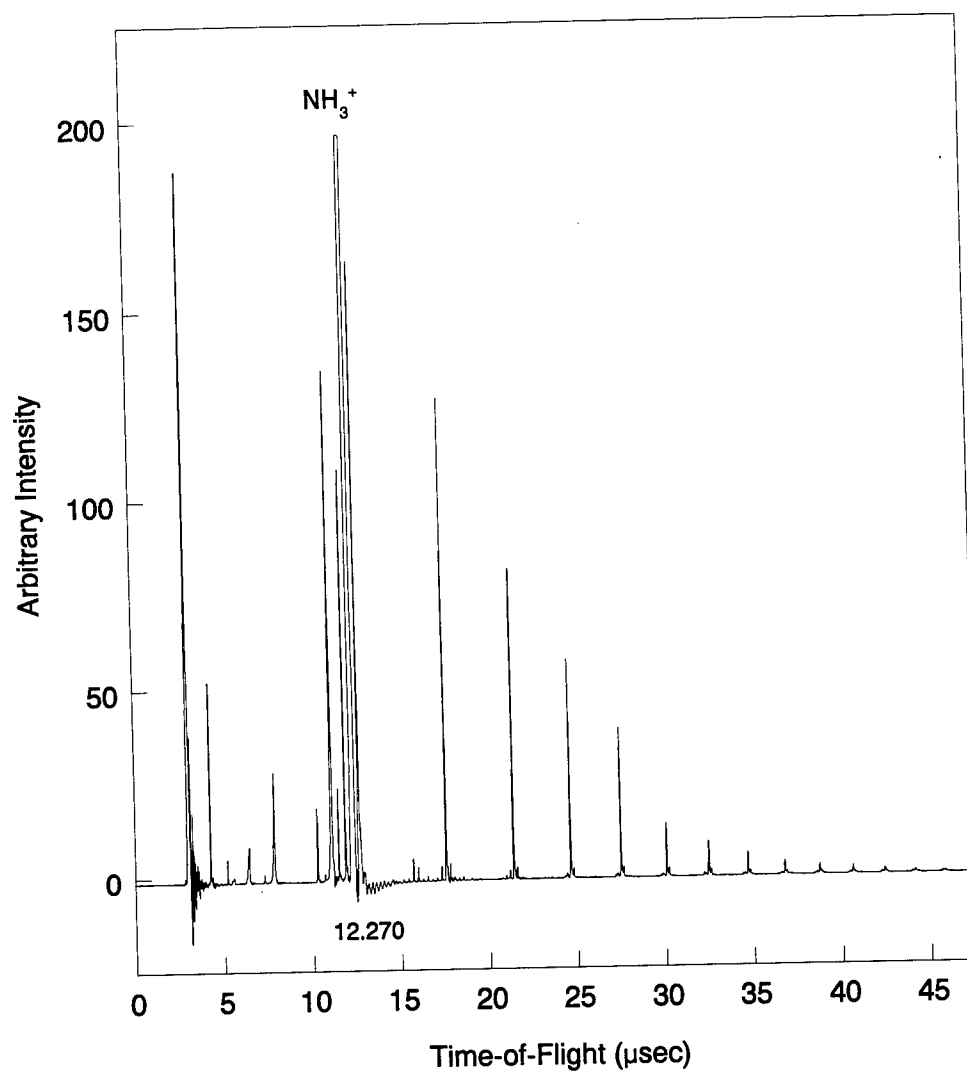


Figure 2-8. The time-of-flight spectrum of ammonia clusters.

where they then encounter a mass reflecting electric field, commonly referred to as a reflectron¹². The reflectron is able to separate metastable ions or to lengthen the time-of-flight of the ions.

As seen in Figure 2-2, the reflectron is a series of thirteen circular stainless steel plates with an outer diameter of 7.5 cm and an inner diameter of 6.25 cm. The openings in the first, second, and last plates are covered with nickel mesh. The first two plates are 1.5 cm apart and the remaining plates are 1.045 cm apart. The plates are separated by alumina spacers.

The first plate is grounded, and the second (U_i) and last plates (U_k) are set at a selected electric potential depending on the experiment conducted. If U_i is higher than the birth potential (U_0), then a hard reflection is used and essentially the time-of-flight is elongated. If U_i is lower and U_k is higher than U_0 , then the metastable ions will be separated. And if U_i is lower and U_k is varied lower than U_0 , then the reflectron is used as an energy analyzer to determine the birth potential of specific ions in the system.

In the studies conducted, a hard reflection was used to simplify the subsequent analysis and U_i was charged to 3700 V.

2.8.4 Microchannel Plate (MCP) Detector

When the particles leave the reflectron they travel another 0.724 m and encounter MCP detector (Galileo FTD 2003). The MCP consists of three circular stainless steel rings with a diameter of 2.54 cm with nickel mesh across the ring. The first two plates are separated by 1.02 cm and the last two are separated by capton insulation (~ 0.2 cm). The first plate is grounded, and the following two are charged at -2300 V and -300 V, respectively. The charge on the plates cause the positive ions to accelerate towards the detector.

2.9 Computations

Driving the collection of all data and calculation of results were computers. The requirements of covariance analysis taxed the capacities of all computer systems involved.

2.9.1 Data Collection

Data for covariance analysis was transferred from the oscilloscope to a P4D-33 Personal Computer (PC) (Gateway 2000) via a PCII General Purpose Interface Bus (GPIB) (National Instruments) interface. In order to expedite the data retrieval process the GPIB was used in a read only mode once the data header information was read. The data was collected in binary format also for expediency. A Version 6 PASCAL (Borland) routine¹² was used to run the interchange and a data transmission of 5 Hz was achieved with this system.

Data was then translated to American Standard Code II (ASCII) to simplify observations and calculational requirements. Translation was conducted on a PC using PASCAL code (Appendix 1)¹³.

2.9.2 Calculation of Covariance

The covariance was calculated using a FORTRAN (IBM) routine (Appendix 2) on the Serial Processor II (SPII) at the Center for Academic Computing at The Pennsylvania State University. The original model routines were run on a Model 550 RISC 6000 system (IBM) within the Castleman Group.

Random access memory (RAM) limitations on the Castleman Group RISC system

forced computations on another system for the full scale calculations. The studies conducted were of 10000 scans with 5000 waveform points each. Because the covariance correlated each of the 5000 waveform points with every waveform point, 25 million points were involved. Using single precision numbers, 200 Mbytes to 300 Mbytes of RAM were required. Only the SPII system was capable of handling this calculation.

Hard drive capacity also played a key role in these calculations. The binary and ASCII input files were 50 Mbytes and 210 Mbytes, respectively. The output files were 500 Mbytes which compressed to less than 200 Mbytes depending on the waveform intensities involved.

References

1. W. C. Wiley, I. H. McLaren, *Rev. Sci. Instrum.* **26**, 1150 (1956).
2. J. A. Valdmanis, R. L. Fork, *IEEE J. Quant. Electronics*, **QE-22** (1), 112 (1986).
3. D. S. Bethune, *Appl. Opt.* **20**, 1897 (1981).
4. A. Yariv, *Optical Electronics*, ed. by M. E. Van Valkenburg, Saunders College Publishing, Philadelphia, 63 (1991).
5. A. Yariv, *Optical Electronics*, ed. by M. E. Van Valkenburg, Saunders College Publishing, Philadelphia, 52 (1991).
- 6a. A. Yariv, *Optical Electronics*, ed. by M. E. Van Valkenburg, Saunders College Publishing, Philadelphia, 54 (1991).
- 6b. O. Svelto, *Principles of Lasers*, ed. D. C. Hanna, Plenum Press, New York, 176 (1989).
7. J. Lowe, *Quantum Chemistry*, Academic Press, San Diego, 79 (1993).
- 8a. S. Wei, W. B. Tzeng, A. W. Castleman, Jr., *J. Chem. Phys* **92** (1), 332 (1990).
- 8b. M. A. Baldwin, P. J. Derrick, ed. R. P. Morgan, *Org. Mass Spectrom.* **11**, 440 (1976).
9. M. Kappes, S. Leutwyler, in *Atomic and Molecular Beam Methods*, Vol. I, ed.: G. Scoles, Oxford University Press, New York, 380 (1988).
10. J. A. Syage, in *Femtosecond Chemistry*, Vol. 2, eds. J. Manz and L. Wöste, VCH Verlagsgesellschaft mbH, Weinheim, 477 (1995).
11. S. Wei, J. Purnell, S. Buzzza, R. J. Stanley, A. W. Castleman, Jr., *J. Chem Phys* **97** (12), 9480 (1992).
12. B. A. Mamyrin, V. I. Karataev, D. V. Shmikk, V. A. Zagulin, *Sov. Phys. JETP* **37** (1), 45 (1973).
13. PASCAL code written by S. A. Buzzza with slight modifications by D. A. Card.
14. PASCAL translation concept originated by S. A. Buzzza.

Chapter 3

Covariance Mapping of Ammonia Clusters: Evidence of the Connectiveness of Clusters with Coulombic Explosion

3.1 Introduction

The study of multi-dimensional correlation of mass spectra has been an evolving topic for the past 32 years¹. The original concept of photoion-photoion correlations (PIPICO)¹⁻⁷ has blossomed into photoion-photoelectron correlations (PEPICO)⁸⁻¹⁵, photoelectron-photoelectron correlations (PEPECO)¹⁶, and photoneutral-photoneutral correlations¹⁷. The addition of a third dimension extended the PEPICO and PIPICO techniques to photoelectron-photoion-photoion correlation methods (PEPIPICO)¹⁸⁻³⁰.

Recognition of the value of these methods has been tempered by realization of their difficulty in implementation. An alternative, but related approach has developed from the statistical concepts of covariance. Codling and coworkers³¹⁻³⁸ demonstrated the power of this method in a series of papers devoted to a study of multicharged processes involving small molecular species such as N₂, N₂O, and CO. The technique requires extensive data analysis, large computational times, and has to date attracted only rather limited attention³¹⁻⁴¹. Despite the computational requirements, the method is very powerful and is an especially attractive one for application to the study of molecular clusters.

The purpose of the present work is to demonstrate the value of covariance analysis through the study of ammonia clusters subjected to intense pulsed radiation in the

femtosecond time domain. The role which clusters play in effecting the formation of species of high charge state has only become recognized very recently⁴²⁻⁴⁷. However, to the best of my knowledge, this is the first observation of the formation of multicharged atoms arising from Coulomb explosion processes which can be directly identified to involve molecular cluster systems. In this chapter, advantage is taken of the concept of covariance analysis to definitively establish the connectiveness of Coulomb explosion with the evolution of various charged species following the ionization of clusters via high intensity laser fields. The value of considering anti-covariance in conjunction with more conventional positive covariance mapping is also discussed.

3.2 Experimental

The equipment used in the present study, which was described earlier in Chapter 2 and by Purnell, et al.⁴⁸, consists of a femtosecond laser ionization system coupled to a molecular beam - reflectron time-of-flight (TOF) mass spectrometer. Briefly, a femtosecond pulse is created when a continuous-wave argon ion laser is impinged on a dye solution of rhodamine 6G in a colliding pulse mode-locked arrangement; the beam is mode-locked with a DODCI dye solution. The beam is amplified with sulforhodamine 640 dye by using the second harmonic of a 10 Hz Nd:YAG laser focused into a six pass Bowtie amplifier, and thereafter with a series of three (2mm/6mm/12mm) Bethune cell amplifiers. Pulse recompression is achieved using gratings. After amplification, the laser

beam is roughly 2.5 mJ/pulse and provides a fluence of about 10^{15} W/cm² at the point where it is focused onto the molecular cluster beam.

Ammonia clusters are produced by expanding ammonia at 2300 Torr through a pulse valve into a vacuum environment (7×10^{-6} Torr), and the laser pulse ionizes a packet of ammonia clusters at the center of the TOF grids. The TOF grids were set at a 1600 V difference and the reflectron was operated in a hard reflection mode whereby the ions were directly reflected to the detector without penetrating into the reflecting electric field of the reflectron. A steep voltage gradient in the TOF lens assembly was purposely employed in this initial study in order to superimpose the dual set of peaks which arise in the Coulomb explosion process, one from the backward and the other from the forward ejected species. Recognizing the additional value to be obtained by undertaking a covariance analysis of associated forward and backward ejected peaks, this has been left as a future research topic. The present study, which represents a test case, incorporated a large number of parent and daughter species and, even with the superimposed peaks, 5000 points needed to be cross correlated for 25 million covariance values. The ion intensity was measured with a microchannel plate detector and the electrical impulses were read via a digital oscilloscope coupled to a personal computer. Neat ammonia (99.98% minimum purity) was used without additional purification.

After a neutral cluster is ionized, it is accelerated in the TOF lens assembly from its point of formation toward lower electric potential. Ions with long lifetimes remain intact until they exit the TOF ionization region and those which are metastable in this time regime are detected as parent masses when the reflectron is operated in the hard reflection

mode. However, ions with short lifetimes decay into smaller fragments prior to departure from the TOF region. All species then traverse a drift region of 2.121 m and are detected at the microchannel plate.

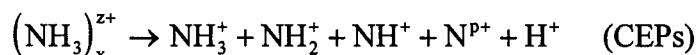
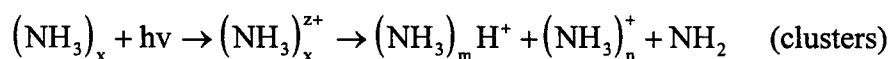
3.3 Results and Discussion

The primary objective of the present study is to identify various associated species ejected in the Coulomb explosion of clusters following their irradiation at high intensity, and to establish the possible existence of competitive versus concerted reaction channels. The species involved in this process are ejected over a broad distribution of angles away from the point of formation, and those which are refocused following backward ejection proceed toward the detector along with ones which are initially ejected in a forward direction. Hence as mentioned above, to explore connectiveness in the Coulomb explosion phenomena, a large potential difference in the birth region was used to preclude the occurrence of split peaks which normally arise due to these two sets of Coulomb explosion particles (CEPs)⁴⁹. Thus, in the arrangement employed, only phenomena occurring within the TOF region can affect the system and cause deviations to an ion's intensity.

In most applications of laser TOF mass spectrometry to cluster studies, advantage is taken of the fact that the ion intensities arising from various processes produce *average intensity* values which can be analyzed and interpreted. However, deviations in the ion intensity do occur because of slight fluctuations in the laser pulse or pulsed nozzle, and

advantage is taken of these fluctuations in implementing the technique of covariance mapping.

In order to discuss the measurements reported herein, an overview of the overall phenomena occurring in the ammonia cluster system must first be given. Briefly, as reported earlier⁴⁹, both singly charged protonated cluster ions as well as nitrogen atoms in various charge states are observed. These observations have been found to be consistent with the following model:



Although the full range of x and z are not precisely known, p is found to range from 1 to 7 and m and n from 1 to 15.

During the course of these experiments, the intensities of the singly charged clusters were found to vary inversely with the intensities of the CEPs. Also, a change in the ratio of their relative abundances was seen when the focal point of the laser was varied. The processes responsible for their production are parallel and competitive, suggesting a rate dependence on the laser fluence. However, as discussed further below, the species do not arise by mutually exclusive reactions.

A rough schematic of the overall reaction and Coulomb explosion phenomena is given in Figure 3-1. (Clearly, this figure is not intended to represent a single reaction surface, but instead to depict the competitive processes operative at different energies.)

By translating the focal point of the laser, the fluence that the clusters experience was changed. As the fluence is varied (by employing different focusing conditions), the energy distributed per neutral cluster can be increased and excites the cluster further; at sufficiently high values this opens the Coulomb explosion channel (State I). Conversely, defocusing distributes the power to more clusters and leads to lower excitation, enabling only singly charged clusters to be formed (State III). A midrange of focusing was selected to explore the threshold region between these processes (State II). The fluctuations in the intensities of the various measurements were exploited to investigate the competitive reaction channels which were first seen during the course of our initial observations employing the use of covariance mapping.

Covariance mapping compares the changes in one measurement with another measurement, via a shot-by-shot analysis. If this involves a large number of repetitive measurements (e.g. 10,000 times), then the results are statistically relevant. Covariance is defined as the deviation in two measurements of two different species, just as the variance is the deviation in two measurements of the same species. Thus the covariance analysis provides a measure of connectiveness between two different parameters, namely two different ionic species in the present case.

Mathematically, the covariance, $C(x,y)$ can be expressed by^{31,50-51}:

$$\begin{aligned} C(x,y) &= \langle (X - \langle X \rangle)(Y - \langle Y \rangle) \rangle \\ &= \langle XY \rangle - \langle X \rangle \langle Y \rangle \end{aligned}$$

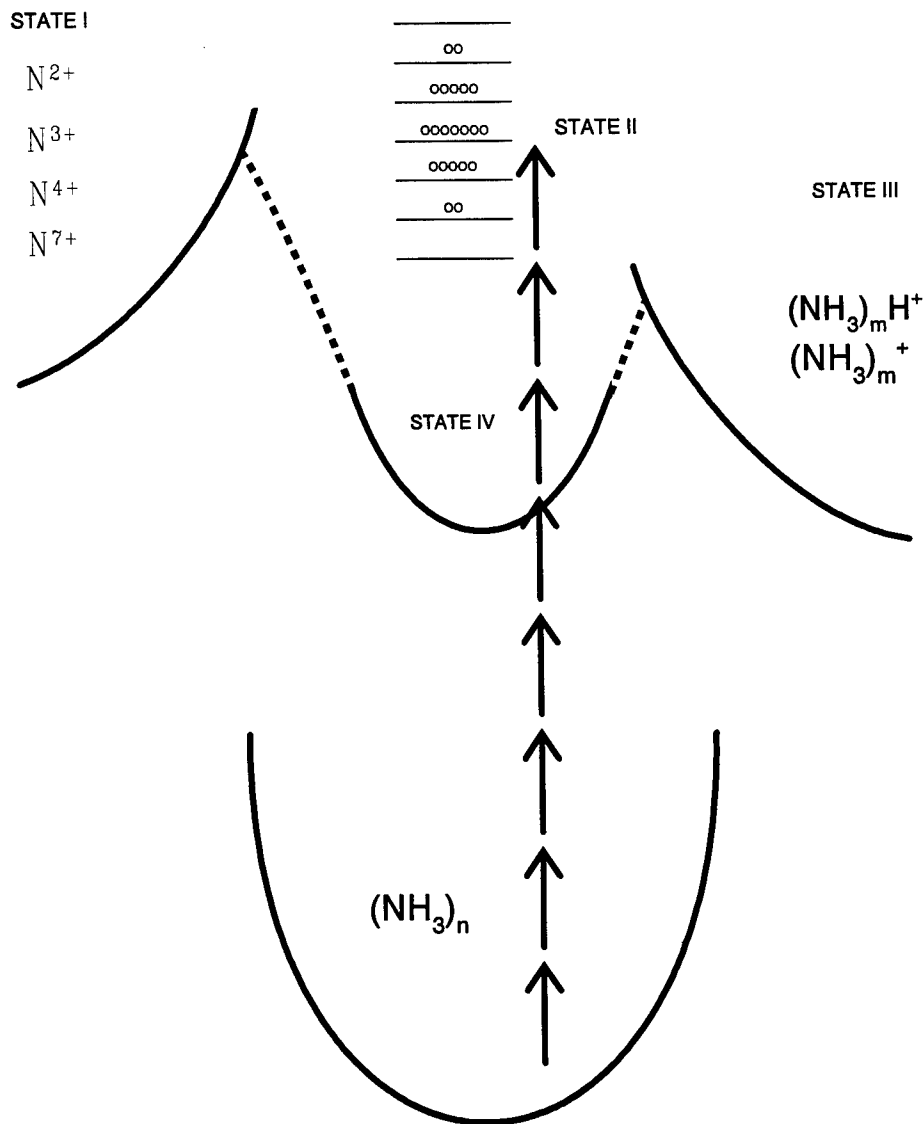


Figure 3-1. Reaction schematic of the excitation of a neutral ammonia cluster to ionization. State I represents an excited state capable of inducing the Coulomb explosion process. State II is the threshold region where moieties of Coulomb exploded particles (CEPs) and singly charged clusters exist together. State III is the ionized cluster state where only singly charged clusters are prevalent as products. State IV is the state in which the cohesive energy of the cluster overcomes the Coulomb repulsion caused by the charges within the cluster.

$$= \frac{1}{N} \sum_{i=1}^N X_i(x) \cdot Y_i(y) - \left[\frac{1}{N} \sum_{i=1}^N X_i(x) \right] \left[\frac{1}{N} \sum_{i=1}^N Y_i(y) \right]$$

where $X_i(x)$ and $Y_i(y)$ represent the intensities at some trace position "i" for a particular ionization period or shot and, for specific species x and y. $C(x,y)$ is termed the covariance⁵⁰. Since $X_i(x)$ and $Y_i(y)$ are the same functions when x equals y, the value of $C(x,x)$ (or $C(y,y)$) is the variance or the square of the standard deviation of the intensity determination.

$$\begin{aligned} C(x,x) &= \frac{1}{N} \sum_{i=1}^N [X_i(x)]^2 - \left[\frac{1}{N} \sum_{i=1}^N X_i(x) \right]^2 \\ &= \sigma_x^2 \end{aligned}$$

Because these are the same functions, a degree of symmetry is found on the x-y axis of all plots. And for plots considering covariances greater than 0, the x-y axis is the variance itself.

The mean function or the trace average is defined as:

$$\overline{X}_i(x) = \frac{1}{N} \sum_{i=1}^N X_i(x)$$

Another closely related term to the covariance is the correlation coefficient, $\rho(x,y)$.

It is a "direct measure" of the similarity of the changes in trace intensity^{33,41,50}, and is defined as:

$$\rho(x,y) = \frac{C(x,y)}{\sqrt{C(x,x) \cdot C(y,y)}} \quad \text{where } |\rho(x,y)| \leq 1$$

If $\rho(x,y)$ equals 1, 0, or -1, the peaks of x and y are considered perfectly correlated, not correlated, or anti-correlated, respectively⁵⁰. Since the variance of a measurement is always a positive quantity, the sign of the correlation coefficient is clearly dependent on that of the covariance. When $\rho(x,y)$ is less than 0, $C(x,y)$ is less than 0, and conversely.

In terms of a chemical reaction, two peaks are obviously correlated if both increase or decrease with each other. On the other hand, two peaks are anti-correlated if one is seen to increase when the other decreases. And if a peak remains unchanged when the other either increases or decreases they are, of course, uncorrelated.

Competitive reactions are ones which deplete a reactive species by two or more channels. Unless two reactions are competitive, the products of all reactions will result in correlations (or no correlations) as opposed to anti-correlations. In the present work, the dependent variable is the decay rate of the multiply charged cluster. However, the rate is a function of the laser intensity or the cluster size (the fluctuating variables in the system). There are two limits to the phenomena under study, namely situations where the species produced become either all CEPs or solely singly charged clusters. Fluences which lead the system to adopt a condition resulting in one of these two limits, eliminates observable coupling between the two measurements (i.e., without a measurement, there are no covariances or correlations) and places the system essentially in one charge state. Snyder,

et al.⁴³ and Wei, et al.⁴⁹ presented data for experiments conducted under conditions corresponding to States I and III; Wei et al. also presented data showing the attainment of a condition leading to stable multi-charged clusters (State IV)⁵².

The abscissa and ordinate inserts of Figures 3-2 and 3-3 is a plot of the TOF mass spectrum for an experiment conducted during the present study and enables an analysis of the covariance map. The time-of-flight mass spectrum represents the conditions of intermediate State II in Figure 3-1. As seen, there are abundant amounts of both CEPs and singly charged clusters.

The center portion of Figure 3-2 is a covariance map where numerical values of $C(x,y)$ greater than 1 are plotted, which enables insight to be gained into the coupling between the reactants or products. The line of symmetry, the x-y axis, and the line defining the variance of the intensity measurements can be seen beginning in the lower left corner. The positive covariance values for this study ranged from 0 to about 3700. Positive values less than 1 corresponded with baseline noise and were ignored. Similarly, the positive correlation data, $\rho(x,y)$, varied from 0 to 1 and values less than 0.1 were ignored as baseline noise.

Voids in the covariance map of Figure 3-2 indicate that no correlation is found between the higher clusters and the CEPs, which implies that they are *not* produced together. Beginning with $(\text{NH}_3)_8\text{H}^+$ and lower order clusters, a steady increase in cross correlation is seen. This clear transition regime where smaller clusters are created along with CEPs would be expected in the threshold region studied.

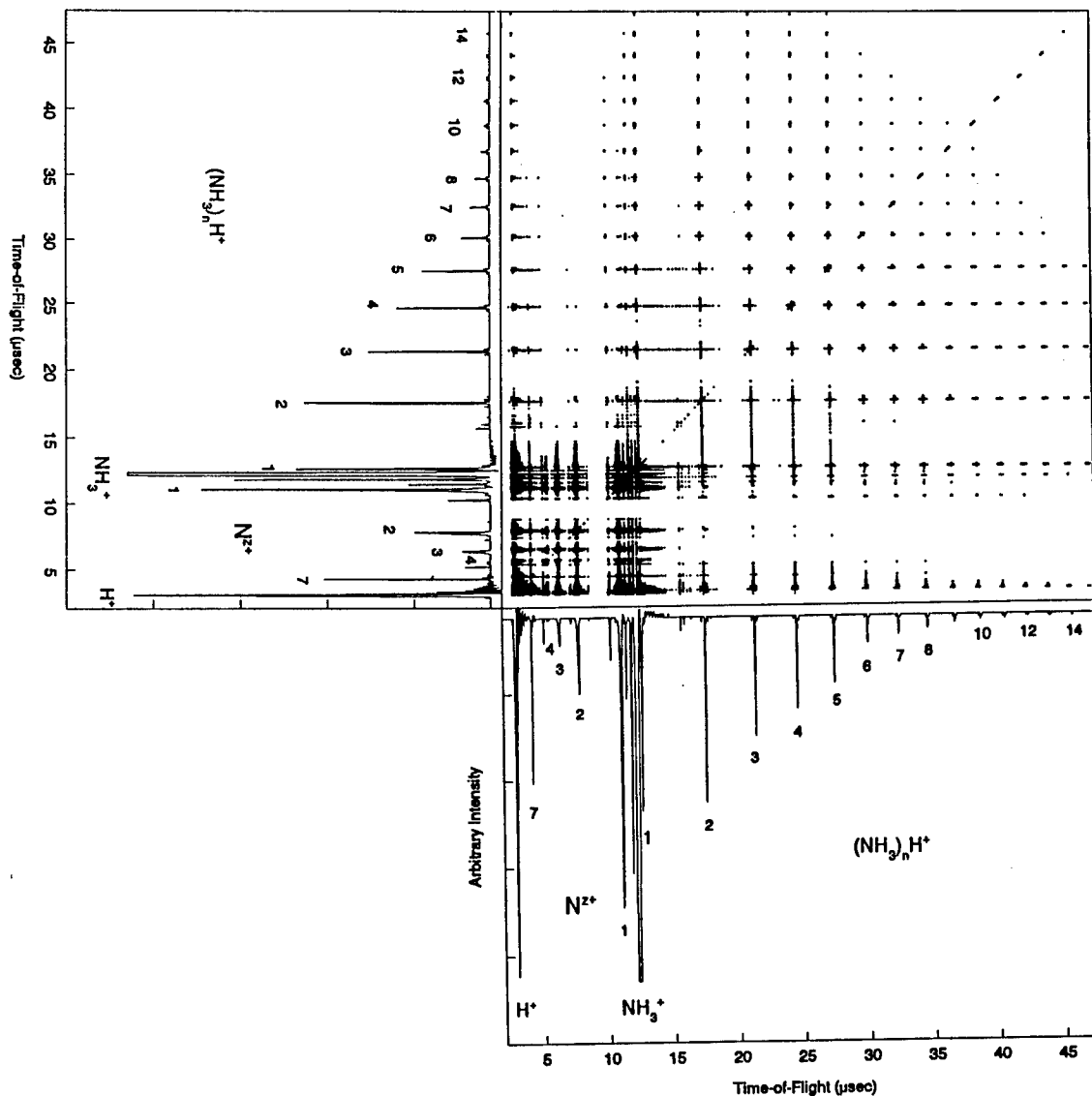


Figure 3-2. Covariance map of ammonia clusters. The abscissa and ordinate display a TOF spectrum of ammonia clusters averaged from 10000 single shot spectra. The center of the figure displays the calculated covariance map as described in the text. Symmetry is clearly visible along the x-y axis starting in the lower left corner. Coupled species are identified by their covariance.

Figure 3-3 is a similar map of covariances less than -1, which represents product coupling through competitive reactions. A similar line of symmetry, the x-y axis, can be seen on this plot as well - albeit since the variance is positive, this line of symmetry is actually a void. Negative covariances ranged from about -1000 to 0. Values between -1 and 0 were indistinguishable from background noise, and hence were ignored. The intense anti-covariance displayed between the higher order clusters and the CEPs, where the void exists in Figure 3-2b, confirms the competitive model presented. Except for Amoruso et al.⁴¹ who studied species evolved from a surface, to the best of my knowledge no other researcher has explicitly explored a system via anti-covariance mapping.

Comparing Figures 3-2 and 3-3, $(\text{NH}_3)_{15}\text{H}^+$ is found to display a covariance with the series $(\text{NH}_3)_n\text{H}^+$, where $1 \leq n \leq 5$, and with H^+ . The absence of any covariance of $(\text{NH}_3)_{15}\text{H}^+$ with the protonated hexamer discounts that any protonated hexamer is produced with $(\text{NH}_3)_{15}\text{H}^+$ through a concerted Coulomb explosion event. These species would be considered uncorrelated with $(\text{NH}_3)_{15}\text{H}^+$. This finding is quite cogent, because otherwise larger singly charged clusters would likely have been found in the study.

A comparison of correlated cluster events with other clusters is made in Figure 3-4, using the peak correlation values. By using the correlation coefficient values, the influence of individual peak intensity is removed and a comparable value is achieved ($-1 \leq \rho(x,y) \leq 1$). Since a higher correlation coefficient value implies a more common connectiveness, the data indicate that all singly charged clusters are more prevalent in their occurrence along with smaller singly charged cluster siblings. The fact that more

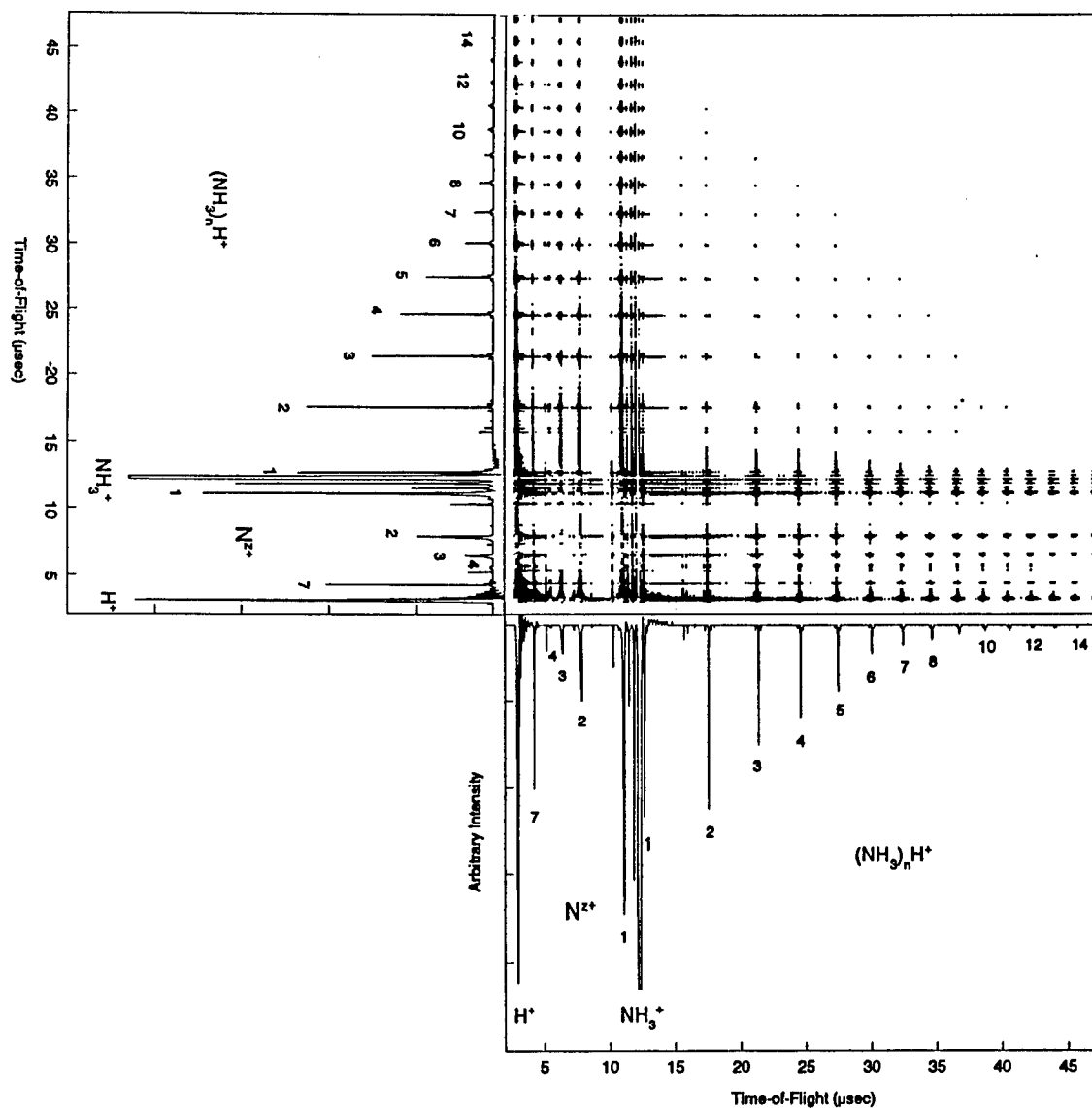


Figure 3-3. Anti-covariance map of Ammonia Clusters. The abscissa and ordinate display a TOF spectrum averaged over 10000 single shots. Proof of the competitive reaction is seen in the CEP cluster covariance field which was absent in the similar domain of Figure 3-2. Although the covariance and anti-covariance maps appear to overlap, each data point (x,y) is distinct and is found on only one map.

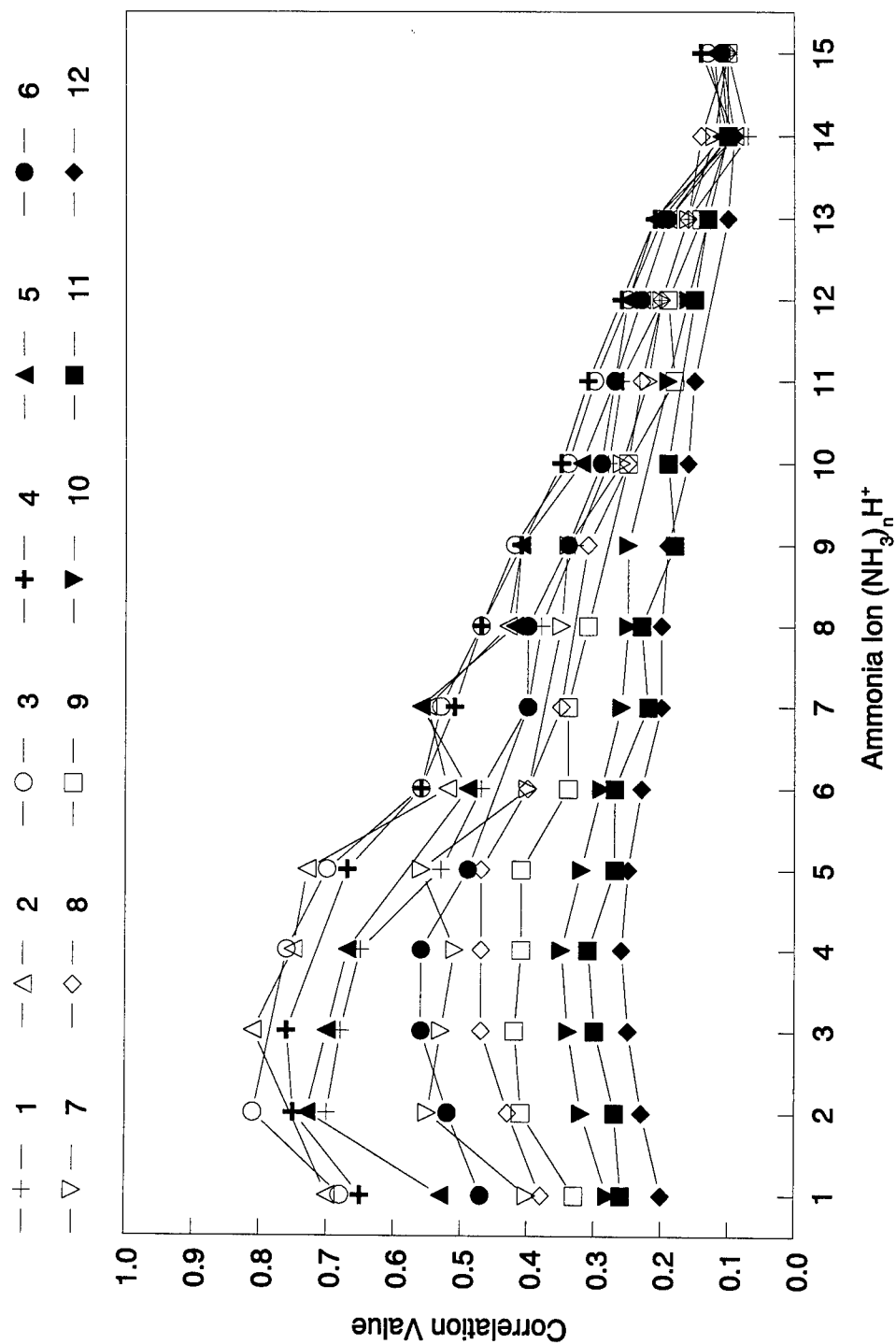


Figure 3-4. Protonated ammonia clusters correlated with other protonated ammonia clusters. Larger singly charged clusters are seen to occur less frequently with similar order singly charged species. A preference of all singly charged clusters occurring with smaller size singly charged clusters is evident. Note self correlations are removed to prevent skewing of the plot at each point.

clusters are favored under these circumstances could imply that they are just more stable in general, that larger clusters are less common under the present beam expansion conditions, or that the processes under study are entropy driven⁵³.

The trend in Figure 3-4 serves to substantiate the inference of a neutral cluster size of at least $(\text{NH}_3)_{21\pm4}$ being involved in the Coulomb explosion process. If the clusters $(\text{NH}_3)_n\text{H}^+$ where $1 \leq n \leq 5$ coexisted along with $(\text{NH}_3)_{15}\text{H}^+$ in each laser shot, then $\rho(x,y)$ would be 1 for every correlation between the species and they would be perfectly correlated. Since $(\text{NH}_3)_{15}\text{H}^+$ occurs, the neutral cluster must be composed of at least $(\text{NH}_3)_{16}$. On the other hand, since $(\text{NH}_3)_{15}\text{H}^+$ is correlated with other clusters, it must occur in coincidence with them. Therefore, the neutral cluster must be at least $(\text{NH}_3)_{21\pm4}$, which would allow for a binary Coulomb explosion event giving rise to these observed species.

The fact that singly charged clusters are sibling products lends credence to the earlier evidence that the instability of the multicharged cluster is due to the existence of an unsymmetric charge distribution^{43,49} at the time of ionization. Clearly, if the charge distribution of the multicharged clusters was perfectly symmetric, then a cluster of $(\text{NH}_3)_{2n+1}^{2+}$ would break up solely into two $(\text{NH}_3)_n\text{H}^+$. Then, the correlation coefficient of this species would be 0 with all other species. Or accounting for an even neutral cluster, $(\text{NH}_3)_{2n}^{2+}$ would break up into $(\text{NH}_3)_n\text{H}^+$ and $(\text{NH}_3)_{n-1}\text{H}^+$, hence, these species would have a correlation coefficient of 1, and display no correlation coefficient with other cluster sizes. These relationships are not seen in Figure 3-4. Thus the multicharged cluster must

have an unsymmetric charge distribution. Logically, increasing the fluence on a neutral cluster to achieve CEPs would also result in an unsymmetric charge distribution.

A plot of the peak correlation values for the sub-monomer species versus the size of the protonated clusters is seen in Figure 3-5. Since the correlation values are negative, the plot represents an anti-correlation comparison. As these species' correlation values approach 0, there is less connectiveness with higher clusters. This demonstrates a gradual trend towards less competition between higher cluster species and CEPs as cluster sizes increase.

3.4 Conclusion

The findings presented herein provide direct evidence of competitive parallel reactions involving singly charged clusters and Coulomb exploded particles that become formed when matter interacts with intense radiation in the ultrafast time region.

The connectiveness of protonated singly charged clusters of different sizes establishes that they arise from the Coulomb explosion of parent clusters of larger size. Although multiply charged clusters smaller in size than those stabilized by their cohesive energy are too unstable to be seen directly in the parent mass distribution, the correlations provided by covariance mapping set lower limits of the size of the neutral cluster species.

The correlations also show good agreement with earlier studies in which kinetic energy measurements pointed to unsymmetric charge distributions giving rise to

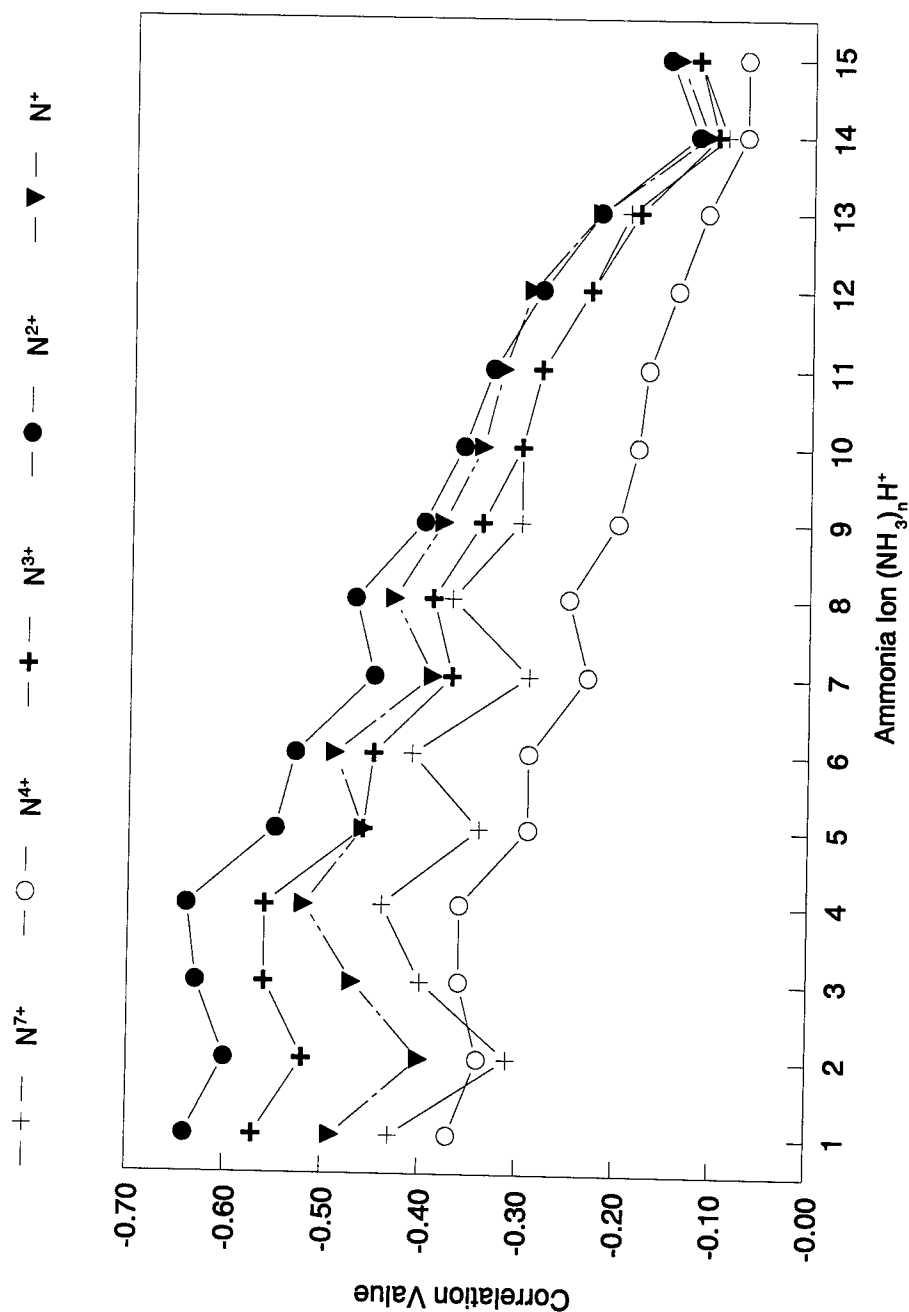


Figure 3-5. Protonated ammonia clusters correlated with multicharged nitrogen ions. Using the correlation coefficient, the multicharged particles are compared with singly charged cluster species without the influence of intensity. Evident is the higher anti-correlation of multicharged species with small size clusters. Although some uncertainties still exist, the peak of mass-to-charge (m/z) 2 in the time-of-flight spectrum was assigned as N^{7+} because of the similarities exhibited in this plot with the other multicharged nitrogen atoms.

split peaks arising from the Coulomb explosion of protonated species⁴⁹. And, except for a few cases, most high charge states show no correlations with singly charged species.

Importantly, the anti-correlation observed between CEPs and larger singly charged clusters presents a new concept of investigating a competitive ionization process. Indeed, the anti-covariance map shows the operative nature of competitive channels in agreement with the model presented in Figure 3-1.

Taken together, the findings support the model due to Wei et al.⁴⁹ that attributes the production of protonated clusters which undergo Coulomb explosion versus the production of CEPs, to a cascading of charge transfer reactions which occur at times short compared to the motion of the nuclei. Finally, the positive covariance seen between the CEPs and small ammonia cluster ions, and the anti-covariance found for the CEPs with the larger clusters further supports the ignition model^{45,47,54} as an important mechanism responsible for the initiation events of multicharge atom formation in clusters, which predicts only a weak dependence on cluster size. This study, and another which appeared recently in literature⁵⁵, show the power of covariance mapping in studying fragmentation in both neutral and ionized molecular clusters.

References

- 1a. M. R. Bruce, C. Ma, R. A. Bonham, *Chem. Phys.* **190**(3,4), 285 (1982).
- 1b. K. E. McCulloh, T. E. Sharp, H. M. Rosenstock, *J. Chem. Phys.* **42**, 3501 (1965).
2. J. C. Creasey, I. R. Lambert, R. P. Tuckett, K. Codling, L. J. Frasinski, P. A. Hatherly, M. Stankiewicz, *J. Chem. Soc., Faraday Trans.* **87**(9), 1287 (1991).
3. J. H. D. Eland, F. S. Wort, P. Lablanquie, I. Nenner, *Z. Phys. D* **4**, 31 (1986).
4. T. Ibuki, A. Hiraya, T. N. Olney, C. E. Brion, C. E. *Chem. Phys.* **203**, 359 (1996).
5. G. Dujardin, S. Leach, O. Dutuit, P. M. Guyon, M. Richard-Viard, *Chem. Phys.* **88**, 339 (1984).
6. G. Dujardin, L. Hellner, D. Winkoun, M. J. Besnard, *Chem. Phys.* **105**, 291 (1986).
7. D. M. Curtis, J. H. D. Eland, *Int. J. of Mass Spect. & Ion Proc.* **63**, 241 (1985).
8. K. Norwood, C. Y. Ng, *Chem. Phys. Lett.* **156**(2,3), 145 (1989).
9. M. R. Bruce, R. A. Bonham, *J. Mol. Structure* **352/353**, 235 (1995).
10. K. Rademann, *Ber. Bunsen-Ges. Phys. Chem.* **93**, 653 (1989).
11. L. Nahon, A. Svensson, P. Morin, *Phys. Rev. A* **43**(5), 2328 (1991).
12. K. Rademann, B. Kaiser, T. Rech, F. Hensel, *Z. Phys. D: At. Mol. and Clusters* **12**, 431 (1989).
13. D. W. Lindle, W. L. Manner, L. Steinbeck, E. Villalobos, J. C. Levin, I. A. Sellin, *J. Elect. Spect. & Rel. Phen.* **67**, 373 (1994).
14. W. Habernicht, K. Müller-Dethlefs, E. W. Schlag, *J. Elect. Spect. & Rel. Phen.* **52**, 697 (1990).
15. J. H. D. Eland, D. Mathur, *Rap. Com. in Mass Spect.* **5**, 475 (1991).
16. G. M. Cross, L. J. Frasinski, L. Zhang, P. A. Hatherly, K. Codling, A. J. Langley, W. Shaikh, *J. Phys. B: Atom. Mol. Opt. Phys.* **27**, 1371 (1994).

17. A. B. Jones, A. L. M. Buxey, P. R. Jukes, J. A. Smith, A. J. Stace, *J. Chem. Phys.* **103**(1), 474 (1995).
18. L. J. Frasinski, M. Stankiewicz, K. J. Randall, P. A. Hatherly, K. Codling, *J. Phys. B: Atom. Mol. Phys.* **19**, L819 (1986).
19. K. Codling, L. J. Frasinski, P. A. Hatherly, M. Stankiewicz, *Phys. Scripta* **41**, 433 (1989).
20. L. J. Frasinski, P. A. Hatherly, K. Codling, *Phys. Lett. A* **156**(5), 227 (1991).
21. P. A. Hatherly, K. Codling, M. Stankiewicz, M. Roper, *J. Phys. B: Atom. Mol. Opt. Phys.* **28**, 3249 (1995).
22. K. Codling, L. J. Frasinski, P. A. Hatherly, M. Stankiewicz, F. P. Larkins, *J. Phys. B: Atom. Mol. Opt. Phys.* **24**, 951 (1991).
23. M. J. Besnard-Ramage, P. Morin, T. Lebrun, I. Nenner, M. J. Hubin-Franskin, J. Delwiche, P. Lablanquie, J. H. D. Eland, *Rev. Sci. Instr.* **60**(7), 2182 (1989).
24. J. H. D. Eland, F. S. Wort, R. N. Royds, *J. Elect. Spect. & Rel. Phen.* **41**, 297 (1986).
25. L. J. Frasinski, M. Stankiewicz, P. A. Hatherly, K. Codling, *Measure. Sci. & Tech.*, 1188 (1992).
26. M. Meyer, J. Lacoursière, M. Simon, P. Morin, M. Larzillière, *Chem. Phys.* **187**, 143 (1994).
27. S. Hsieh, J. H. D. Eland, *Rap. Com. Mass Spect.* **9**, 1261 (1995).
28. M. Stankiewicz, P. A. Hatherly, L. J. Frasinski, K. Codling, D. M. P. Holland, *J. Phys. B: Atom. Mol. Opt. Phys.* **22**, 21 (1989).
29. P. A. Hatherly, M. Stankiewicz, L. J. Frasinski, K. Codling, M. A. MacDonald, *Chem. Phys. Lett.* **159**(4), 355 (1989).
30. K. Codling, L. J. Frasinski, P. A. Hatherly, M. Stankiewicz, *Phys. Scripta* **41**, 433 (1990).
31. L. J. Frasinski, K. Codling, P. A. Hatherly, *Science* **246**, 1029 (1989).
32. L. J. Frasinski, K. Codling, P. A. Hatherly, *Phys. Lett. A* **142**(8,9), 499 (1989).

33. K. Codling, L. J. Frasinski, *Contemporary Phys.* **35**(4), 1994, 243 (1994).
34. L. J. Frasinski, M. Stankiewicz, P. A. Hatherly, G. M. Cross, K. Codling, A. J. Langley, W. Shaikh, *Phys. Rev. A* **46**(17), R6789 (1992).
35. L. J. Frasinski, P. A. Hatherly, K. Codling, M. Larsson, A. Persson, C-G. Wahlström, *J. Phys. B: Atom. Mol. Phys.* **27**, L109 (1994).
36. K. Codling, L. J. Frasinski, *J. Phys. B: Atom. Mol. Phys.* **26**, 783 (1993).
37. P. A. Hatherly, M. Stankiewicz, K. Codling, L. J. Frasinski, G. M. Cross, *J. Phys. B: Atom. Mol. Phys.* **27**, 2993 (1994).
38. K. Codling, C. Cornaggia, L. J. Frasinski, P. A. Hatherly, J. Morellec, D. Normand, *J. Phys. B: Atom. Mol. Phys.* **24**, L593 (1991).
39. M. R. Bruce, L. Mi, C. R. Sporleder, R. A. Bonham, *J. Phys. B: Atom. Mol. Phys.* **27**, 5773 (1994).
40. M. Stankiewicz, L. J. Frasinski, G. M. Cross, P. A. Hatherly, K. Codling, A. J. Langley, W. Shaikh, *J. Phys. B: Atom. Mol. Phys.* **26**, 2619 (1993).
41. S. Amoruso, V. Berardi, N. Spinelli, R. Velotta, M. Armenante, F. Fuso, M. Allegrini, E. Arimondo, *Appl. Surf. Sci.* **86**, 35 (1995).
42. J. Purnell, E. M. Snyder, S. Wei, A. W. Castleman, Jr., *Chem. Phys. Lett.* **229**, 333 (1994).
43. E. M. Snyder, S. Wei, J. Purnell, S. A. Buzza, A. W. Castleman, Jr., *Chem. Phys. Lett.* **248**, 1 (1996).
44. E. M. Snyder, D. A. Card, D. E. Folmer, A. W. Castleman, Jr. in *Resonant Ionization Spectroscopy 1996*, ed. N. Winograd and J. E. Parks, American Institute of Physics, Woodbury, 379 (1997).
45. E. M. Snyder, S. A. Buzza, A. W. Castleman, Jr., *Phys. Rev. Lett.* **77**(16), 3347 (1996).
46. K. Boyer, B. D. Thompson, A. McPherson, C. K. Rhodes, *J. Phys. B: At. Mol. Opt. Phys.* **27**, 4373 (1994).

47. C. Rose-Petruck, K. J. Schafer, C. P. Barty, J. *Applications of Laser Plasma Radiation II, SPIE* **272**, 2523 (1995).
48. J. Purnell, S. Wei, S. A. Buzza, Castleman, A. W., Jr *J. Phys. Chem.* **97**, 12530 (1993).
49. S. Wei, J. Purnell, S. A. Buzza, E. M. Snyder, A. W. Castleman, Jr., *Femtosecond Chemistry*; VCH Verlagsgesellschaft mbH, Weinheim **2**, 449 (1995).
50. J. W. Goodman, *Statistical Optics*, John Wiley & Sons, New York, 17 (1985).
51. I. Noda, *Appl. Spect.* **47**(9), 1329 (1993).
52. S. Wei, J. Purnell, S. A. Buzza, R. J. Stanley, A. W. Castleman, Jr., *J. Chem Phys.* **97**(12), 9480 (1992).
53. C. Bréchnignac, P. Cahuzac, M. de Frutos, N. Kebaïli, A. Sarfati, V. Akulin, *Phys. Rev. Lett.* **77**(2), 251 (1996).
54. I. Last, I. Schek, J. Jortner, *Energetics and Dynamics of Coulomb Explosion of Highly Charged Clusters*, To be published.
55. P. Jukes, A. Buxey, A. B. Jones, A. Stace, *J. Chem. Phys.* **106**(4), 1367 (1997).

Chapter 4

Future Directions

4.1 Introduction

The result of nearly every experiment or investigation is a conclusion and many unanswered questions. The development of covariance mapping ended no differently.

Some of the remaining challenging questions are:

(1) Are all species on the covariance map products or are several reactants in a feeddown process?

(2) Can covariance mapping be used to further explore the Coulomb explosion process - especially its mechanism?

(3) Will studies involving metastable decay reveal further information?

(4) What is the kinetic process governing Coulomb explosion in clusters?

Undoubtedly, there are many other questions one could pursue. However these are issues I would like to pursue in my future research.

4.2 Proposal

In order to explore these questions, a plan of action is appropriate. Some of the questions are not mutually exclusive of each other.

4.2.1 Exploring the Coulomb Explosion Process.

In order to explore questions 1 and 2, a slight modification of the current apparatus is necessary. Utilizing a second laser system and a mass gate, a system of known cluster size may be explored. As shown in Figure 4-1, one laser ionizes the neutral cluster and after identification, the mass gate is used to selectively filter a desired species out of the spectrum. By synchronizing the laser pulses, a second laser will be used along the time-of-flight to further ionize the selected species.

If the Coulomb explosion process leading to multiply charged particles is dependent on clusters, then further addition of energy to the non-cluster species should not result in multiply charged species. However, if the clusters are integral in the process, addition of energy to cluster species should result in multiply charged species.

Using the technique of covariance mapping, the controversy of symmetric or unsymmetric decay of the general Coulomb explosion process¹⁻⁶ should be resolved. By mass selecting a cluster cation and observing the decay in a covariance map, the symmetry of the map around the cluster cation species should unambiguously end the dispute. If the decay is symmetric, then only a covariance between the cation cluster and up to two progeny should be visible (one if the parent was an odd numbered parent to begin with). On the other hand, if the decay is unsymmetric, then an array of covariances between the cation cluster and many children should be visible. Because the reactant involved in the system is known (selected via mass gate), the product and reactant covariances should be separated.

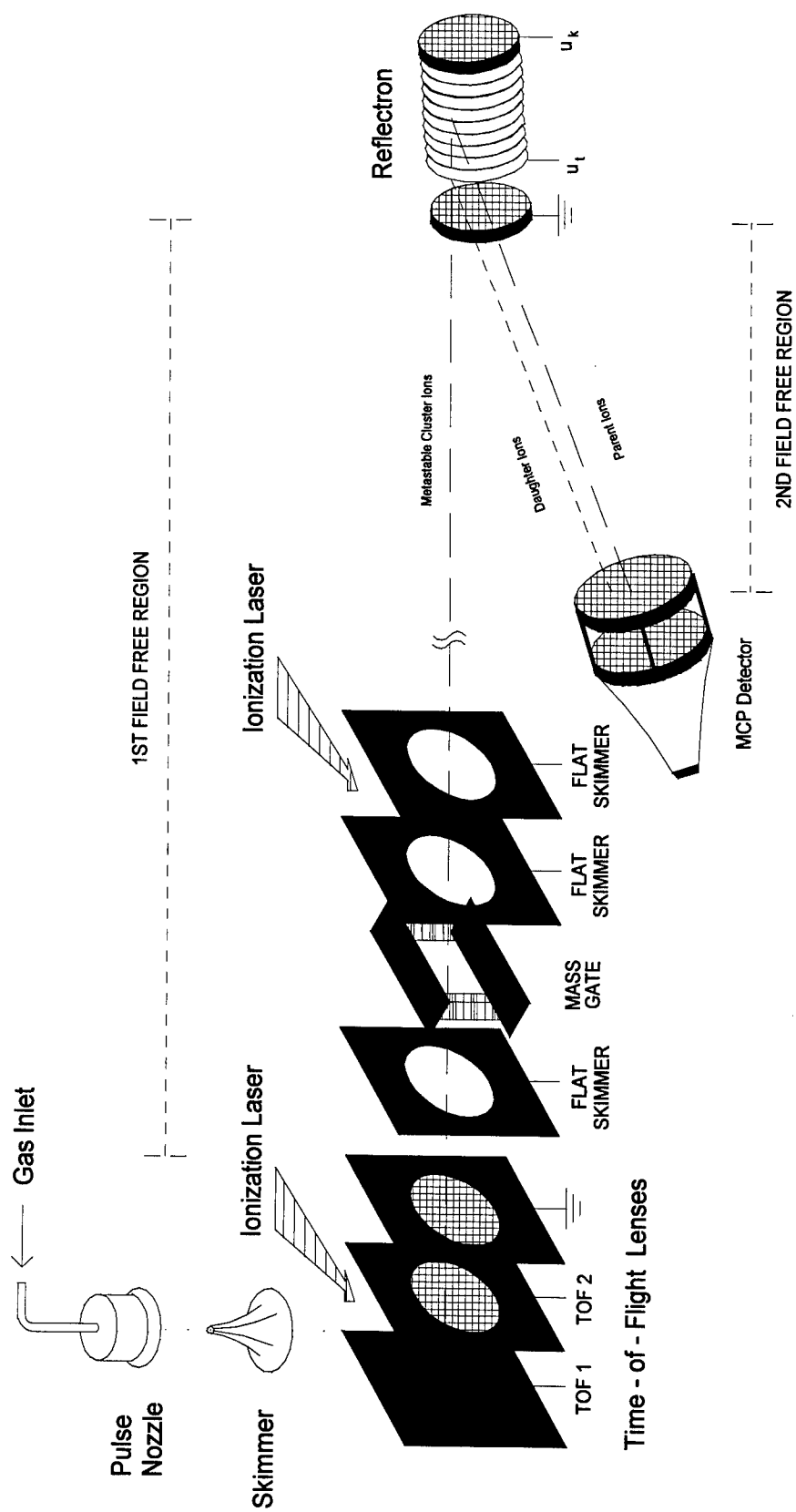


Figure 4-1. The Reflectron Time-of-Flight Mass Spectrometer (R-TOFMS) with Mass Gate

4.2.2 Covariance Mapping and Metastable Decay.

Without initiating any equipment changes, metastable processes could be explored. Results of the expected covariance map would be resolution of whether daughter ions would correlate with the daughters released prior to exiting the TOF region. If correlation is found, the results should replicate cut-off experiments conducted with a reflectron and demonstrate further the mechanisms which occur within the TOF region during Coulomb explosion.

4.2.3 The Kinetic Process Governing Coulomb Explosion.

Utilizing the setup shown in Figure 2-2 and placing a lower field gradient on the plates, further resolution of the ammonia system should develop. The placement of a lower field gradient allows a greater separation of the forward and backward ions. The covariance map of this system would be exponentially more complicated than that presented in Figures 3-2 and 3-3.

Results expected would be a closer bracketing of the neutral cluster (within the deviations of the pulse nozzle and laser), a model of decay for the Coulomb explosion process, and perhaps a better understanding of the process as it evolves upon impinging a laser on the cluster.

4.3 Conclusion

Without question, covariance mapping is an intriguing tool to interrogate systems and resolve them unambiguously. Future work in this area should be increasingly more common as covariance maps are better understood and computer processes are upgraded to accommodate the requirements of covariance maps.

References

1. J. Purnell, E. M. Snyder, S. Wei, A. W. Castleman, Jr., *Chem. Phys. Lett.* **229**, 333 (1994).
2. E. M. Snyder, S. Wei, J. Purnell, S. A. Buzza, A. W. Castleman, Jr., *Chem. Phys. Lett.* **248**, 1 (1996).
3. E. M. Snyder, D. A. Card, D. E. Folmer, A. W. Castleman, Jr. in *Resonant Ionization Spectroscopy 1996*, ed. N. Winograd and J. E. Parks, American Institute of Physics, Woodbury, 379 (1997).
4. K. Boyer, B. D. Thompson, A. McPherson, C. K. Rhodes, *J. Phys. B: At. Mol. Opt. Phys.* **27**, 4373 (1994).
5. C. Rose-Petruck, K. J. Schafer, C. P. Barty, *J. Applications of Laser Plasma Radiation II, SPIE* **272**, 2523 (1995).
6. I. Last, I. Schek, J. Jortner, *Energetics and Dynamics of Coulomb Explosion of Highly Charged Clusters*, To be published.

Appendix

Computer Programs

A.1 Introduction

Covariance mapping is computationally intensive. The magnitude of covariance mapping requirements has literally impeded the growth and development of it as a working tool of mass spectrometry. There has been, over the course of its development, the emergence of computers capable of crunching through the tremendous repetition of calculations.

The following routines were specifically written to generate the covariance between two pieces of data. Several have seen numerous major revisions since the onset of this study. The versions listed are merely the latest version, but by no means a final version. Each requires specific data input and output files to be designated before they may be used. The input and output files within the routines are the latest to be translated.

A.2 PASCAL Routines

Two routines written in PASCAL were used in the development of the final covariance product. The first was a modified version of Femtoscan.exe¹ and the second, Covar.exe.

A.2.1 Femtoscan.exe

Femtoscan.exe and its interrelated programs were slightly modified.

Femtoscan.exe was used in the rare read only configuration. The program set the oscilloscope into single trigger mode, received the waveform header information, and then read the waveform information in binary for the prescribed number of shots. Binary was used because the data transmission could not keep up with the laser repetition rate (10 Hz). An average rate of 5 Hz was achieved.

A.2.2 Covar.exe

Covar.exe was written to translate the binary data into ASCII code. To expedite the process and also to minimize the datafile sizes, the quantized oscilloscope readings were used instead of the scaled and translated readings. By using the quantized readings (0-255), the input filesize was reduced by a factor of 6 (e.g., 1.2 Gbytes versus 210 Mbytes). The data translation time was decreased to around 60%. Although not specifically compared, using the quantized readings unquestionably reduced the FORTRAN execution times as well.

Covar.exe uses the same variables and arrays used in Femtoscan.exe by design and some by the requirements of PASCAL. The current version of Covar.exe is:

{ \$N+ }

PROGRAM Covar;

{** This program converts raw covariance datafiles into an ASCII datafile to be used by a FORTRAN program for covariance calculations. The data is stored in the following format:

- 1) Information about the waveform (34 BYTES)
- 2) Raw waveform data for first shot (BYTE length determined by the field WfInfo.WF_Pts-1)
- 3) Raw waveform data for second shot

.
.
.

n+1) Raw waveform data for nth shot ***}

USES DOS, CRT;

TYPE CovarianceInfo = RECORD

Wf_Pts : WORD; {2 BYTES}
 Hor_Interval : DOUBLE; {8 BYTES}
 Hor_Offset : DOUBLE; {8 BYTES}
 Vert_Gain : DOUBLE; {8 BYTES}
 Vert_Offset : DOUBLE; {8 BYTES}
 END; {34 BYTES TOTAL}

VAR

DATAFILE : FILE; { * Untyped datafile *}
 TEXTFILE : TEXT; { * Converted ASCII File *}
 WfInfo : CovarianceInfo; { * RECORD of waveform information *}
 NumberOfShotsRead, { * Blocks of data transformed *}
 NumberOfShots, { * Blocks of data to be transformed *}
 DataFileSize, { * Total size of datafile *}
 i,j,k : LONGINT;
 TempExtended, { * Temporary variable *}
 TempInteger : INTEGER; { * Temporary variable *}
 TempString : STRING; { * Temporary variable *}
 DataArray : ARRAY[1..20002] OF BYTE; { * Data storage *}

BEGIN

ASSIGN(DATAFILE,'d:\dennis\961120\nv20cv2.SPC');

```

RESET(DATAFILE,1); {*** The datafile is opened to the beginning of the file. ***}
DataFileSize := FILESIZE(DATAFILE);
BLOCKREAD(Datafile,WFInfo,SIZEOF(WFInfo));
{*** The first 34 bytes of the datafile are read. The field WFInfo.WF_Pts is 2 greater
    than the experimental parameters because the trace point before and after the
    experimental points are picked up in the total. Although the field is 2 greater than
    the experiment, only the point preceeding the experimental points is recorded.
    Thus the first datafile point is not considered for experimental purposes and is
    discarded. ***}

NumberofShots := TRUNC((DataFileSize-SIZEOF(WFINFO))/(WFInfo.WF_Pts-1));

{*** The total number of shots in the covariance file is calculated. The header length
    (34 bytes) is subtracted first. The remaining datafile is a multiple (number of
    shots + 1) of the datafile size. ***}

ASSIGN(TEXTFILE,'d:\dennis\961120\nv20cv2.ASC');
REWRITE(TEXTFILE);
STR(NumberofShots, Tempstring);
WRITELN(TEXTFILE, Tempstring);
STR((WFInfo.WF_Pts-2),Tempstring);
WRITELN(TEXTFILE, Tempstring);

NumberofShotsRead := 0;

REPEAT
    INC(NumberofShotsRead);
    APPEND(TEXTFILE);
    BLOCKREAD(DataFile,DataArray,WFInfo.Wf_Pts-1);

    FOR i := 2 TO WFINFO.Wf_Pts-1 DO BEGIN
        TempInteger := DataArray[i] {SHL 8};
        WRITE(TEXTFILE,TempInteger{ div 256}:4);
        IF ((i-1) mod 10) = 0 THEN WRITELN(TEXTFILE,"");
    END;
    CLOSE(TEXTFILE);
UNTIL NumberofShotsRead = NumberofShots;

{*** The REPEAT loop proceeds UNTIL all the shots have been transformed and
    placed in the ASCII datafile. ***}

CLOSE(DATAFILE);

```

END.

{ \$M 45000,0,25000 }

A.3 FORTRAN Routines

Two routines were developed for computing the covariance and filtering through the 25 million data points involved. The routine which calculated the covariance was Covar.f and the filter routine was Optim.f.

A.3.1 Covar.f

Covar.f was modeled² and written for a maximum of 10000 runs with 5000 waveform points. Single precision variables are designated to limit the RAM requirements. RAM requirements for this routine are a little more than 400 Mbytes. Moving to double precision would double the RAM requirements. Full scale calculations could only be conducted on SPII system at the CAC. Special compilation was required to execute the routine because of the RAM requirements.

The input datafile size was 210 Mbytes and the output files for the covariance and the correlation matrices were 500 Mbytes each. Average run times were around 1 day.

The current version of Covar.f is:

PROGRAM COVAR

```
REAL*4 CBAVG(5000),CA(5000,5000), C(5000,5000), RHO
INTEGER*4 I,J,K,III,JJJ,N,O,A(10000,5000),CASUM,CBSUM
```



```

OPEN (UNIT=8,FILE='nv20cv2.asc',STATUS='OLD')
OPEN (UNIT=10,FILE='cnv20cv2.asc',STATUS='UNKNOWN')
OPEN (UNIT=15,FILE='tnv20cv2.asc',STATUS='UNKNOWN')
C
C   THIS PROGRAM IS MODELED ON THE FRANSINSKI, CODLING,
C   HATHERLY PAPER FOUND IN SCIENCE, 24 NOV 89.
C
C   DATA IS INTENDED TO BE INPUT FROM A DATA FILE, COVARIN,
C   WHICH IS EXTERIOR TO THIS PROGRAM.
C
C   READ THE NUMBER OF DATA RUNS, N, WHERE N <= 10000.
C
C   READ (8,997) N
C
C   READ THE NUMBER OF DATA POINTS PER RUN, O, WHERE O <= 10000.
C
C   READ (8,992) O
C
C   READ THE INTENSITY DATA, A(I,J), WHERE I IS THE DATA RUN AND J IS
C   THE TIME OF FLIGHT OF THE ION.
C
C   DO 100 I = 1, N
C       DO 99 J = 1, O, 10
C           READ (8,998) (A(I,J+K),K=0,9)
99   CONTINUE
100  CONTINUE
C       CLOSE (UNIT=8)
C
C   CALCULATE THE PRODUCT SUMMATION, CA(I,J), OVER THE DATA
C   RUNS AT POINT I AND J.
C
C   DO 200 J=1, O
C       DO 199 K=1, O
C           CASUM=0
C           DO 198 I=1, N
C               CASUM=A(I,J)*A(I,K)+CASUM
198  CONTINUE
C           CA(J,K)=CASUM*1.0/N
199  CONTINUE
200  CONTINUE
C
C   CALCULATE THE AVERAGE INTENSITY, CBAVG(J), SUMMED OVER THE
C   ENTIRE RUN.

```

```

C
298 DO 300 JJ=1,O
    CBSUM=0
    DO 299 II=1, N
        CBSUM=A(II,JJ)+CBSUM
299 CONTINUE
    CBAVG(JJ)=CBSUM*1.0/N
    WRITE (15,993) JJ, CBAVG(JJ)
300 CONTINUE
    CLOSE (UNIT=15)
C
C CALCULATE THE COVARIANCE OF THE THE POINTS I AND J.
C
    DO 400 III=1, O
        DO 399 JJJ=1, O
            C(III,JJJ)=CA(III,JJJ)-CBAVG(III)*CBAVG(JJJ)
            WRITE (10,996) III,JJJ,C(III,JJJ)
399 CONTINUE
400 CONTINUE
    CLOSE (UNIT=10)
C
C CALCULATE THE CORRELATION COEFFICIENT BETWEEN THE POINTS
C I AND J.
C
OPEN (UNIT=14,FILE='pnr20cv2.asc',STATUS='UNKNOWN')
    DO 500 I=1, O
        DO 499 J=1, O
            RHO=C(I,J)/(C(I,I)*C(J,J))**.5
            WRITE (14,996) I,J,RHO
499 CONTINUE
500 CONTINUE
    CLOSE (UNIT=14)
C
C FORMAT STATEMENTS
C
992 FORMAT (I4)
993 FORMAT (I5,2X,F9.4)
996 FORMAT (I5,I5,F9.2)
997 FORMAT (I5)
998 FORMAT (10I4)
1000 FORMAT (1X,10E4.0)
999 STOP
    END

```

A.3.2 Optim.f

Optim.f was written as a companion routine to Covar.f. Because of the long run times of Covar.f, placing a filter within it required that the routine be rerun each time. Instead the results were scanned using the output from Covar.f. Filter run times were reduced to several minutes in some cases.

The current version of Optim.f splits the covariance matrix in two and places negative values less than -1 into one file and positive values greater than 1 into another file. Values between -1 and 1 were indistinguishable from background noise and were ignored.

Optim.f is easily modified to allow selection of any particular layer within the covariance matrix. This routine has been modified dozens of times to this end. The current version of Optim.f is:

```

PROGRAM OPTIM
  REAL*4 VAR
  INTEGER*4 I,J,K,L,M,N,O,IX,IY
  INTEGER*8 ICOUNT, ICOUNT1
C
C THE EXACT VALUE OF THE ICOUNT VARIABLE CAN BE CALCULATED BY
C DIVIDING THE DATAFILE SIZE BY 20. THE FILTER SHOULD BE RESET
C SOMEWHAT HIGHER THAN IT'S ORIGINAL VALUE FROM THE
C EXECUTING FILE THAT THE DATAFILE WAS CREATED FROM.
C
  FILTER1=1.0
  FILTER2=-1.0
  ICOUNT=25000000
  ICOUNT1=0
C

```

```
OPEN (UNIT=9,FILE='cnv20cv2.asc',STATUS='OLD')
OPEN (UNIT=10,FILE='cnv20cv2.ant',STATUS='UNKNOWN')
OPEN (UNIT=11,FILE='cnv20cv2.cor',STATUS='UNKNOWN')
```

C

```
DO 100 I=1, ICOUNT
  READ (9,990,END=101) IX,IY,VAR
  IF (VAR.LE.FILTER2) GO TO 98
  IF (VAR.LT.FILTER1) GO TO 99
  WRITE (10,991) IX,IY,VAR
  GO TO 99
98  WRITE (11,991) IX,IY,VAR
99  ICOUNT1=ICOUNT1+1
100 CONTINUE
101 CLOSE (UNIT=9)
    CLOSE (UNIT=10)
    CLOSE (UNIT=11)
```

C

```
990 FORMAT (I5,I5,F9.2)
991 FORMAT (I5,I5,F9.0)
999 STOP
    END
```

References

1. S. A. Buzza, PhD Dissertation, The Pennsylvania State University, December 1995.
2. L. J. Frasinski, K. Codling, P. A. Hatherly, Science, 1029 (1989).

VITA

Dennis A. Card

EDUCATION

Bachelor of Science in Chemical Engineering, University of Missouri, Rolla, 1985
Masters of Science in Chemistry, The Pennsylvania State University

PROFESSIONAL EXPERIENCE

1982-1985 Undergraduate Teaching Assistant, University of Missouri, Rolla
1985 Research Chemist, Rockford Coatings
1985-Present Chemical Officer, United States Army

AWARDS

1981-1985 Army Reserve Officers Training Corps Scholarship
1983-1985 Lewis B. Young Scholarship
1985 Graduate Summa Cum Laude

PROFESSIONAL SOCIETIES

1985-Present Tau Beta Pi (Professional Engineering Fraternity)
1990-Present Association of the United States Army
1993-Present Missouri Board for Architects, Professional Engineers, and Land Surveyors (Engineer-in-Training)